Chapter 3

On the Life Cycle of Individual Contrails and Contrail Cirrus

ULRICH SCHUMANN

Deutsches Zentrum für Luft- und Raumfahrt, Institut für Physik der Atmosphäre, Oberpfaffenhofen, Germany

ANDREW J. HEYMSFIELD

National Center for Atmospheric Research, Boulder, Colorado

ABSTRACT

The life cycle of individual (initially line shaped) contrails behind aircraft and of contrail cirrus (aged contrails mixed with other ice clouds) is described. The full contrail life cycle is covered, from ice formation for given water, heat, and particulate emissions; to changes in the jet, wake, and dispersion phases; through final sublimation or sedimentation. Contrail properties are deduced from various in situ, remote sensing, and model studies. Aerodynamically induced contrails and distrails are explained briefly. Contrails form both in clear air and inside cirrus. Young contrails consume most of the ambient ice supersaturation. Optical properties of contrails are age and humidity dependent. Contrail occurrence and radiative forcing depends on the ambient Earth–atmosphere conditions. Contrail cirrus seems to be optically thicker than assessed previously and may not only increase cirrus coverage but also thicken existing cirrus. Some observational constraints for contrail cirrus occurrence and radiative forcing are derived. Key parameters controlling contrail properties—besides aircraft and fuel properties, ambient pressure, temperature, and humidity—are the number of ice particles per flight distance surviving the wake vortex phase, the contrail depth, and particle sedimentation, wind shear, turbulence, and vertical motions controlling contrail dispersion. The climate impact of contrails depends among other things on the ratio of shortwave to longwave radiative forcing (RF) and on the efficacy with which contrail RF contributes to surface warming. Several open issues are identified, including renucleation from residuals of sublimated contrail ice particles.

1. Introduction

Contrails (condensation trails) form behind aircraft as line-shaped cirrus clouds, with high concentrations of small ice particles compared to other cirrus (see Fig. 3-1). Contrails may form as ''exhaust contrails'' from water and particles emitted by the aircraft engines (Schumann 1996) or as ''aerodynamic contrails'' forming because of adiabatic cooling near curved surfaces of the aircraft (Gierens et al. 2009; Kärcher et al. 2009). Distrails (dissipation trails) and aircraft-induced cloud holes may also form (Heymsfield et al. 2011). Contrails are mostly short-lived but may persist for many hours when forming in ice-supersaturated air (Minnis et al. 1998). Individual contrails deform with time, often merge with other contrails and cirrus, and eventually form ''contrail cirrus'' (Schumann 2002). Contrail cirrus can be distinguished from other cirrus only when traced back to the formation process (Graf et al. 2012). Early studies discussed the visibility and detection aspects of contrails (aufm Kampe 1943; Brewer 1946; Appleman 1953; Ryan et al. 2011), and these studies contributed to the detection of ice supersaturation, contrail persistence, the dryness of the stratosphere, the Brewer–Dobson circulation (Brewer 2000), and hollow ice particles (Weickmann 1945). The climate impact got more attention later (Penner et al. 1999). The mean radiative forcing (RF) from contrails is likely positive, possibly contributing to global warming (Boucher et al. 2013). In contrast to

Corresponding author e-mail: Ulrich Schumann, ulrich.schumann@dlr.de

DOI: 10.1175/AMSMONOGRAPHS-D-16-0005.1

FIG. 3-1. Contrail types. (a) Exhaust contrail (photo by Josef P. Williams; Unterstrasser et al. 2012). (b) Aerodynamic contrail (photo by Dieter Klatt; Gierens et al. 2011). (c) Aircraft-induced lines and holes in supercooled liquid clouds (cloud-top temperatures −35° to −25°C); section of image with blue border lines, near northwest corner of Texas (29 Jan 2007, NASA, Jeff Schmaltz, MODIS Rapid Response Team). (d) Contrail visible shortly behind B747-400 engines, 38 000 ft, −61°C, 28 May 2004; photo by Robert Falk. (e) ''Soot cirrus'' observed at DLR, Oberpfaffenhofen, 0905 UTC 3 Nov 2013. (f) Persistent contrails west of lake Ammersee, Germany, photo by C. Koenig, DLR, 23 Jun 2002. (g) Persistent contrails and contrail cirrus, a false-color *NOAA-12* AVHRR image, 5 Apr 1995, processed by DLR.

many other climate effects discussed for aviation, contrail cirrus is observable (see Fig. 3-1f). This review summarizes the present understanding of contrail cirrus and identifies some open questions. The insight gained may be of relevance for cirrus research, contrail climate assessment, and mitigation (including optimized aircraft and engines, changed routing, and alternative fuels), not discussed here (Fuglestvedt et al. 2010; Lee et al. 2010; Grewe et al. 2014a; Brasseur et al. 2016). The paper describes first the formation and properties of ''individual contrails.'' This term is used instead of ''line-shaped contrails'' because it is not clear when a line-shaped contrail ends. The second part describes contrail cirrus.

2. Individual contrails

a. Mean contrail properties

Since contrails start as line-shaped clouds, unlike most other cirrus clouds, special integral properties are used. Just as other cirrus particles, each contrail particle has an individual mass m_i, projected particle cross-section area A_i, habit, and orientation (see the appendix for a list of symbols). These properties plus the phase, composition, temperature, and wavelength determine the optical extinction efficiency $Q_{\text{ext},i}$ and other microphysical and optical properties of each particle (Hansen and Travis 1974). Integral properties peculiar to contrails are the geometrical cross-section area A_c, and the total crystal number N_{ice}, total extinction EA, and total ice mass I per flight distance:

$$N_{\text{ice}} = \sum n_i = A_c n_{\text{ice}}, \tag{3-1}$$

$$EA = \sum n_i Q_{\text{ext},i} A_i = Q_{\text{ext}} N_{\text{ice}} \pi r_{\text{area}}^2 = A_c \varepsilon = \tau W, \quad \text{and} \tag{3-2}$$

$$I = \sum n_i m_i = (4\pi/3)\rho_{\text{ice}} N_{\text{ice}} r_{\text{vol}}^3 = \text{IWC}\ A_c. \tag{3-3}$$

Here, the local and the volume-mean ice particle concentrations n_i and n_{ice}, extinction ε, and ice water content IWC occur, with mean extinction efficiency Q_{ext} and ice-bulk density ρ_{ice}, besides optical depth τ and contrail width W. The summation sums over all ice particles in the contrail cross section. The above equations also define the volume and area-mean radius of the contrail particles, r_{vol} and r_{area}. By tradition, the definitions are set up so they

equal the geometrical radius in the idealized case of monodisperse spherical particles (Hansen and Travis 1974). The effective radius r_{eff} is defined by the ratio of mean particle volume to cross-section area, $r_{\text{eff}} = 3IQ_{\text{ext}}/(4\rho_{\text{ice}}EA)$. Again the factor (¾) enters for consistency with a hypothetical sphere radius. By definition, $r_{\text{vol}}/r_{\text{eff}} = r^2_{\text{area}}/r^2_{\text{vol}}$. The ratio $C = r_{\text{vol}}/r_{\text{eff}}$ depends on ice particles sizes and habits and needs to be determined empirically; $C \leq 1$ if the ice particles were spherical. Measured data collected for contrails show that $C \approx 0.7 \pm 0.3$ varies during the lifetime of the contrails and depends on ambient humidity (Schumann et al. 2011).

The aircraft wake evolution is traditionally divided into the jet, vortex, and dispersion regimes (Hoshizaki et al. 1975). After a roll-up phase (Misaka et al. 2015) overlapping with the jet regime, the vortex regime exhibits two phases: a first phase of a coherent counterrotating vortex pair and a second phase with rapid hydrodynamic vortex breakup and subsequent turbulent dissipation (Gerz and Holzäpfel 1999; Paoli and Shariff 2016).

b. Formation of exhaust contrails

1) FORMATION CONDITIONS

Exhaust contrails form during the jet phase because of engine emissions of water and particles [mainly soot, i.e., impure carbon particles resulting from incomplete combustion of hydrocarbon fuels (Bond et al. 2013; Petzold et al. 2013)] acting as cloud condensation nuclei (CCN). The emissions depend on fuel mass flow m_F per flight distance (all-engine contribution) and on emission indices (EI) for exhaust species [gaseous or particulate (PEI); mass and number of emitted species per mass of fuel burned]. A fraction $\eta = F/(Qm_F)$ of the specific combustion energy Q is used to propel the aircraft (depending on m_F and thrust F), so that the fraction $(1 - \eta)$ of Q appears in the young exhaust jet plume, partly in form of kinetic energy of the jets (Schumann 1996). The remainder heats the aircraft wake later, when all motions induced by the aircraft are dissipated. The term η is known as ''overall propulsion efficiency'' in engine technology (Penner et al. 1999). Contrails form when the exhaust gases exceed liquid saturation at least for a short time. Humidity (measured by partial vapor pressure) and heat (measured by temperature) in the exhaust plume decrease during mixing of the warm and humid exhaust gases with cool ambient air at about the same rate, along a straight mixing line in Fig. 3-2a. Relative humidity is the ratio of the partial pressure of water vapor in the exhaust relative to the saturation vapor pressure for given temperature. From the Clausius–Clapeyron equation, the saturation pressure follows a curve in this figure. Therefore, relative humidity is higher inside the plume than at engine exit and in ambient air. Maximum potential supersaturation is reached when the plume temperature reaches liquid maximum (LM) T_{LM}. The plume humidity exceeds liquid saturation at least briefly when the ambient air temperature T is below a threshold temperature [liquid critical (LC)] T_{LC}. Temperature T_{LC} depends on ambient relative humidity RH (for liquid saturation) and a parameter G,

$$T < T_{\text{LC}} = T_{\text{LM}} - \frac{p_{\text{sat}}(T_{\text{LM}}) - \text{RH}p_{\text{sat}}(T_{\text{LC}})}{G},\ \frac{dp_{\text{sat}}(T_{\text{LM}})}{dT} = G,\ \frac{dp_{\text{sat}}(T_{\text{LM}})}{dT} = G, \tag{3-4}$$

with saturation pressure $p_{\text{sat}}(T)$ over liquid water. From these equations, $T_{\text{LM}}(G)$ and $T_{\text{LC}}(G, \text{RH})$ can be determined by Newton iteration or from approximate solutions (Schumann 2012). The parameter G covers the dependency of the threshold on ambient pressure p, and EI_{H2O}, Q, and η, defined above, and the specific heat capacity c_p of air, and molar masses M_{H2O} and M_{air} of water and air. This Schmidt–Appleman criterion (SAC; Schumann 1996) does not consider phase changes and the process of ice production. It assumes quick conversion of kinetic energy from the engine jet into internal energy and simultaneous mixing of heat and water vapor between the exhaust jet and cloud-free ambient air. Within the accuracy of temperature and humidity measurements, the SAC has been verified experimentally (Busen and Schumann 1995; Schumann et al. 1996; Jensen et al. 1998b; Schumann et al. 2000). The measurements confirmed earlier findings that ice saturation is insufficient for formation of visible contrails. Figures 3-2b–f show probabilities of contrail formation properties for the global air traffic of 2006 and meteorology from the European Centre for Medium-Range Weather Forecasts (ECMWF). The plots show the frequency of flight conditions (p, T, η, RHi), in relation to threshold conditions. Potentially, without phase changes, 90% of the contrails experience liquid supersaturation ($\text{RH}_{\text{LM}} - 1$) higher than 5% (up to 230% for low T), mainly near plume temperatures of 230 K for ambient temperatures near 220 K.

2) CONTRAIL ICE FORMATION

For conventional jet fuels and engines, contrail ice particles are frozen water droplets containing some soot or other CCN material (Kärcher et al. 1996; Wong and Miake-Lye 2010). Because of potentially high liquid supersaturation, liquid droplets form even on less hygroscopic CCN in the young contrail (Koehler et al. 2009). This is supported by particle refractive index measurements in young contrails suggesting internal mixtures of

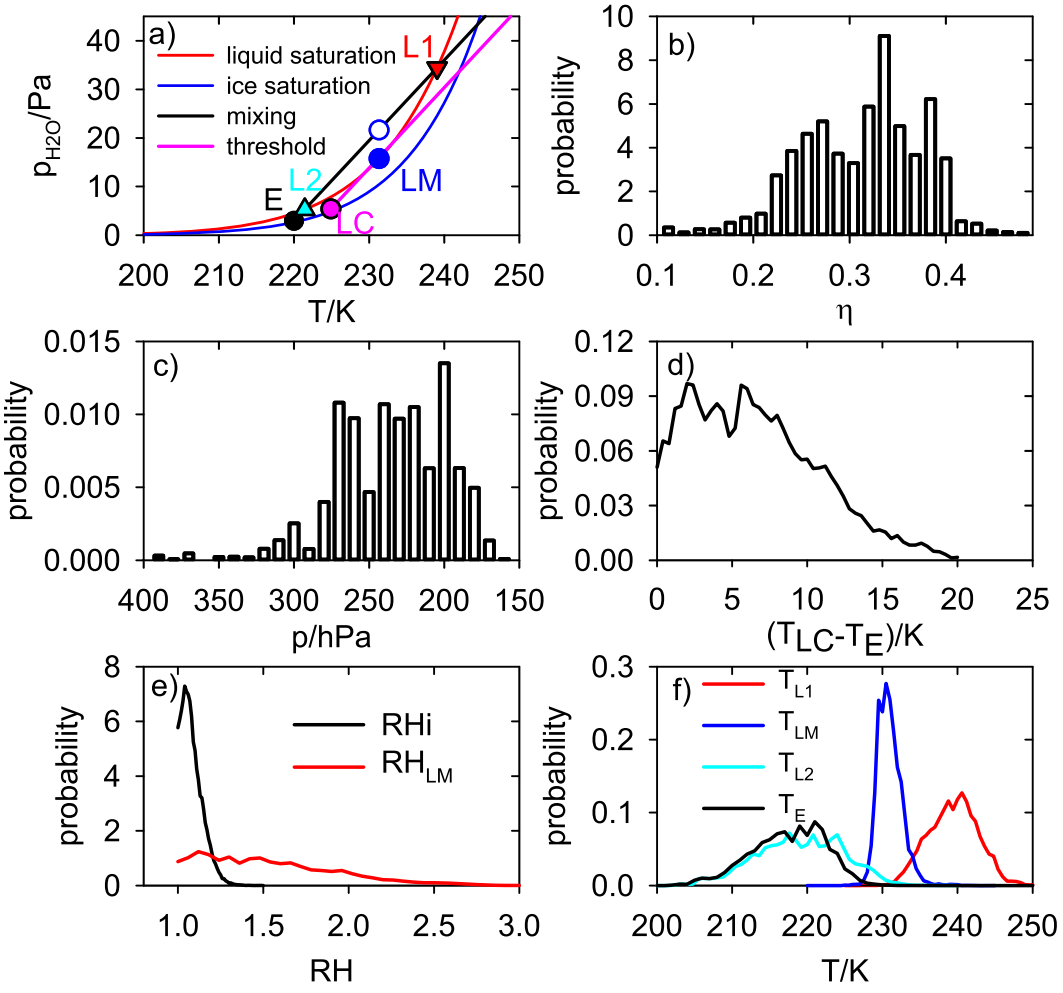

FIG. 3-2. (a) Contrail formation principle (for $G = 1.65\,\mathrm{Pa\,K^{-1}}$), identifying the points of maximum liquid saturation (LM), first liquid saturation (L1), and last liquid saturation (L2) for given environment (E, $T_E = 220$ K, RHi = 1.1) and SAC threshold conditions (LC). Probability density functions of persistent contrail formation thermodynamics for 2006 air traffic from the FAA's Aviation Climate Change Research Initiative (ACCRI) project and NWP data from ECMWF: (b) overall propulsion efficiency η; (c) pressure; (d) threshold temperature difference above ambience; (e) relative humidity RHi over ice and potential RH_{LM} over liquid saturation at LM without phase changes; (f) temperature at L1, LM, L2, and E [colors as in (a)].

soot in contrail ice particles (Kuhn et al. 1998). A significant reduction of interstitial nonvolatile particles has been observed when contrails form, indicating that exhaust soot indeed participates in ice formation (Schröder et al. 1998). Besides soot, volatile aerosol forming in the engine exhaust plume may also contribute to ice nucleation, in particular for low soot particle emissions ($<10^{14}\,\mathrm{kg^{-1}}$) and low ambient temperatures (<213 K; Kärcher and Yu 2009; Wong and Miake-Lye 2010). High concentrations of volatile aerosol have been observed (Fahey et al. 1995). The effect of fuel sulfur content is smaller than expected initially (Schumann et al. 1996; Jurkat et al. 2011).

For ~10% of all contrails, the ambient temperature is only 1 K below the threshold temperature. Here, details of the CCN become important (Kärcher et al. 2015). Ice particles form either by homogeneous freezing of the liquid droplets (not involving ice nuclei) or heterogeneously by ice nuclei (Wong and Miake-Lye 2010). The fraction f_c of soot particles forming droplets decreases with soot loading because of the increased competition for the vapor available for condensation (Kärcher et al. 1996; Paoli et al. 2013). For alternative fuels, with different aerosol and aerosol precursor emissions, ice may form by freezing of water droplets forming on soot (possibly heterogeneously) for high soot concentrations and from volatile material (homogeneously) for less soot (Rojo et al. 2015).

The number N_{ice} of ice particles per flight distance forming in the young contrail depends also on the time available for condensation and for ice formation. Without freezing, the contrail particles would soon evaporate

even in ice-supersaturated but liquid-subsaturated air. The liquid droplets freeze quickly after formation because of low temperature and high relative humidity in the contrail. Liquid saturation may persist more than 10 s along the plume axis but <0.1 s at the outer edge of the exhaust plume. Faint contrails become visible to passengers already close to the engine exit for low temperature (see Fig. 3-1d) and about a wing span after engines under threshold conditions (Busen and Schumann 1995). In the interior of the well-mixed plume, condensation starts many wing spans behind the engine (Schumann et al. 1996; Paoli and Shariff 2016). Outside the plume center, mixing proceeds far quicker, leaving less time for condensing water during liquid supersaturation. Ice particles at the outer edge of contrails experience higher relative humidity and less competition for the available moisture than in the center, thereby getting larger than in the contrail interior, as observed (Petzold et al. 1997; Heymsfield et al. 1998).

3) MIXING AND PLUME DILUTION

Mixing of the exhaust jet plume depends on interaction between the jet and the wake vortices in the roll-up phase (Khou et al. 2015), with similar characteristic time scales of mixing and condensation (Wong and Miake-Lye 2010; Paoli et al. 2013). The wide range of time scales may be important for contrail formation from alternative fuels.

Mixing can be expressed in terms of a dilution ratio $N_{\rm dil}$ (Schumann et al. 1998). Here, $N_{\rm dil}$ is the mass of air inside the plume per mass of fuel burned, both per flight distance. This definition avoids any dependence on air–fuel ratio in the engine that arises if dilution is defined relative to engine exhaust mass flow. Measurements have shown that the dilution of tracers near the plume center follows approximately

$$N_{\rm dil} \approx 7000(t/t_0)^{0.8}, \tag{3-5}$$

where $t_0 = 1$ s. This result is a bit surprising because it is independent of aircraft and atmosphere scales, but has been confirmed by various measurements and applied successfully for estimates of aircraft exhaust concentrations and plume ages (Schäuble et al. 2009; Rojo et al. 2015).

4) SOOT EMISSIONS

Since other emissions scale with fuel consumption m_F per flight distance and with an emission index, it makes sense to define an apparent particle emission index $\mathrm{PEI_{ice}}$ such that $N_{\rm ice} = \mathrm{PEI_{ice}} m_F$. If each ice particle would share the same amount of exhaust water, in ice-saturated ambient air, and after cooling to ambient temperature, then the volume-mean radius would be

$$r_{\rm vol} \approx [3\mathrm{EI_{H2O}}/(4\pi\rho_{\rm ice}\mathrm{PEI_{ice}})]^{1/3}, \tag{3-6}$$

implying $r_{\rm vol} \approx 0.67\,\mu$m for $\mathrm{EI_{H2O}} = 1.24$ and $\mathrm{PEI_{ice}} = 10^{15}\,\mathrm{kg^{-1}}$, with $\rho_{\rm ice} \approx 917\,\mathrm{kg\,m^{-3}}$ as ice-bulk density (if without air bubbles). This simple analysis shows the high importance of $\mathrm{PEI_{ice}}$ for contrail properties. Since we expect $\mathrm{PEI_{ice}} = f_c \mathrm{PEI_{soot}}$, we need to know f_c and the soot number emission index.

Soot formation, mainly from fuel aromatics, is fuel, engine, and power dependent (Moore et al. 2015). Lower fuel aromatics (naphthalene) content reduces $\mathrm{PEI_{soot}}$ (Braun-Unkhoff and Riedel 2015). Modern engines tend to emit less soot than older ones (Lee et al. 2010). The mass of soot particles $m_{\rm soot}$, relating $\mathrm{EI_{soot}} = m_{\rm soot}\mathrm{PEI_{soot}}$, increases with thrust setting (Timko et al. 2010). The mass-specific soot emission index $\mathrm{EI_{soot}}$ is traditionally determined from ground tests (using smoke number measurements), and more recently from ground-based direct measurements (Timko et al. 2010; Boies et al. 2015). $\mathrm{EI_{soot}}$ at cruise can be estimated from ground-based measurements and engine parameters (Peck et al. 2013). Stettler et al. (2013) show that current methods deriving aircraft soot mass emissions from smoke number data may underestimate the mass emissions by about a factor of 3, partly because smaller particles contribute little to the smoke number measurement. From the few experimental data points from in situ measurements behind cruising civil subsonic aircraft, in particular during the former Subsonic Aircraft Contrail and Cloud Effects Special Study (SUCCESS; Anderson et al. 1998) and SULFUR projects (Petzold et al. 1999; Schumann et al. 2002), one finds $\mathrm{PEI_{soot}}$ of 0.2 to $10 \times 10^{15}\,\mathrm{kg^{-1}}$ and $m_{\rm soot} \approx (4 \pm 2) \times 10^{-20}$ kg. More information is required on soot number emissions ($\mathrm{PEI_{soot}}$) and on the fraction f_c of soot acting as CCN for given contrail formation conditions.

5) NUMBER OF ICE PARTICLES FORMED

Ice particles and soot particles under cruise conditions are difficult to measure simultaneously. Part of the soot gets scavenged by contrail ice (Schröder et al. 1998), and therefore ice and soot are measured behind aircraft separately in dry or wet plumes (Brock et al. 2000). The SULFUR project showed that the number of ice particles in young contrails is comparable to the number of soot particles emitted from the engines. $\mathrm{PEI_{ice}}$ increases slightly (by a factor of <2) when fuel sulfur content increases from 6 to $2800\,\mu\mathrm{g\,g^{-1}}$. The effective $\mathrm{PEI_{ice}}$ derived from in situ contrail ice particle measurements (Schröder et al. 2000) with dilution from Eq. (5) varies between 10^{14} and $10^{15}\,\mathrm{kg^{-1}}$ (Schumann 2005). During a more recent field experiment, the Contrail and Cirrus

Experiment (CONCERT; Voigt et al. 2010), ice particle concentrations were measured in contrails behind various airliners for contrails of a few minutes' age. The derived $\mathrm{PEI}_{\mathrm{ice}}$ values vary between 0.7 and 7.2 $\times$ $10^{14}\,\mathrm{kg}^{-1}$, with the higher values in the secondary wake above the sinking primary wake (Jeßberger et al. 2013). The results were compared with $\mathrm{PEI}_{\mathrm{soot}}$ values derived from ground measurements for given flight conditions, and it was found that $\mathrm{PEI}_{\mathrm{ice}}$ is larger than the $\mathrm{PEI}_{\mathrm{soot}}$ (Schumann et al. 2013b). This suggests that aircraft either emit more soot particles suitable for contrail formation than estimated or that particle losses are less than predicted. The effect of alternative fuels on particle emissions and the formation of contrails has been investigated since May 2014 within the Alternative-Fuel Effects on Contrails and Cruise Emissions (ACCESS II) and Emission and Climate Impact of Alternative Fuels Experiment (ECLIF) projects (B. Anderson and H. Schlager, American Geophysical Union, 2015, personal communication). In summary, $N_{\mathrm{ice},0}$ in the young contrail can be estimated from the soot emissions and the fuel consumption per unit flight distance,

$$N_{\mathrm{ice},0} = \mathrm{PEI}_{\mathrm{ice}} m_F = f_c \mathrm{PEI}_{\mathrm{soot}} m_F . \tag{3-7}$$

c. Aerodynamic contrails, distrails, and cloud holes

Aerodynamic contrails show nicely colored iridescent line clouds (Fig. 3-1b). Contrail iridescence was observed for contrails early (Sassen 1979). Aerodynamic contrails form from intense adiabatic cooling in the airflow over aircraft wings (Gierens et al. 2009). The colors in the aerodynamic contrail are explained by the rapid growth of nearly monodisperse particles, which are visible when observed close to the sun (Kärcher et al. 2009). Only recently it was shown that most of the visible particles form from homogeneous droplet nucleation (Jansen and Heymsfield 2015). The meteorological conditions for aerodynamic contrail formation have been examined in a case study and globally (Gierens et al. 2011; Gierens and Dilger 2013). Visible aerodynamic contrails occur in an altitude range between roughly 540 and 250 hPa, preferentially at temperatures between −20° and −50°C, and for RH > 80% (Jansen and Heymsfield 2015). The number of ice particles formed in aerodynamic contrails is not well known, but likely smaller than for exhaust contrails (Kärcher et al. 2009). Often exhaust and aerodynamic contrails form simultaneously (see Figs. 3-1a,b). Aerodynamically induced ice particles may cause inadvertent seeding of ice in supercooled clouds. This explains observed aircraft-induced holes in clouds at temperatures between −10° and −20°C (see Fig. 3-1c). These holes may contribute to snow precipitation near airports (Heymsfield et al. 2011). Distrails (dissipation trails) are visible occasionally from ground and in satellite images as linear gaps in clouds (Duda and Minnis 2002). Distrails may result from exhaust or from mixing induced by aircraft (Scorer and Davenport 1970). For nice distrail photos and historical remarks, see Pedgley (2008).

d. Contrail wake vortex phase

Wake vortices depend on aircraft properties including aircraft wing span s, mass M, and true airspeed V, and on atmosphere parameters, such as air density ρ, Brunt–Väisälä frequency N_{BV}, turbulence dissipation rate ε_t, and gravity g, which together define wake vortex scales:

$$b_0 = \frac{\pi}{4} s, \quad \Gamma_0 = \frac{gM}{b_0 \rho V}, \quad t_0 = \frac{2\pi b_0^2}{\Gamma_0}, \quad w_0 = \frac{b_0}{t_0},$$
$$N_{\mathrm{BV}}^* = N_{\mathrm{BV}} t_0, \quad \varepsilon_t^* = \frac{(\varepsilon_t b)^{1/3}}{w_0}. \tag{3-8}$$

Here, b_0 measure the lateral distance between the vortex lines, Γ the integral vortex circulation; and t_0, w_0, N_{BV}^*, and ε_t^* are the related time, velocity, stratification, and dissipation scales, respectively. The wake vortex forms because of aerodynamics: Lift balances aircraft weight by inducing downward momentum on the air behind the aircraft wing. Lift requires circulation (Kutta–Joukowski theorem). Circulation is the integral of velocity along a line around the wing and equals the integral of the open surface bounded by that line (Stokes theorem). Vorticity departs with the flow from the wing rear edges or the wing tips depending on the lift distribution along the wing (Anderson 2010). Some distance behind the aircraft, a vortex pair forms, which sinks with mean speed w_0 initially, until buoyancy becomes important or until hydrodynamic instabilities have grown sufficiently to cause a sudden breakup into dissipating turbulence. The jet regime ends ~4–40 wing spans behind the aircraft, depending on speed, engine number, and engine positions, when the exhaust jets and the freshly formed contrails got captured in the wake vortex system (Gerz and Ehret 1996). Depending on this interaction, most of the exhaust gets captured in the primary wake vortex (Greene 1986). Part of the exhaust stays outside and above the sinking primary wake and forms the "secondary wake" (Misaka et al. 2012; Holzäpfel 2014; Paoli and Shariff 2016).

Only a fraction f_s of the ice crystals formed in the jet survives the transition from contrail formation until final decay of the wake vortices (Sussmann and Gierens 1999). Any initial ice supersaturation in the contrail gets

reduced rapidly by deposition of the vapor excess on the many ice particles in the jets, before the vortex has descended much and reached its lowest altitude. The sinking vortex experiences adiabatic heating (Greene 1986), which causes a slight local subsaturation around the ice particles, even sensitive to the Kelvin effect, that is, a reduction of saturation pressure depending on particle curvature and surface tension (Naiman et al. 2011; Lewellen 2012). As a consequence, the smaller ice particles sublimate and the number of ice particles decreases (Lewellen and Lewellen 2001). The secondary wake contains fewer but larger ice particles and binds more ice water because of quicker mixing with ambient humid air and less heating by adiabatic sinking. At low ambient humidity, the primary wake may sublimate after some time while the secondary wake persists longer (Sussmann and Gierens 2001). The fraction f_s of ice particles surviving the wake vortex depends on temperature and humidity, and on the wake vortex scales, and also on the number and size of ice particles formed in the jet phase. The fraction can be estimated from a parameterization based on several recent large-eddy simulation (LES) studies (Unterstrasser 2016). As a consequence, any decrease in particle emissions causes a less than linear decrease in the number of ice particles. It would be important to validate these model results by measurements.

A set of data of individual contrails for ages from seconds to hours is compiled in Fig. 3-3 from previous in situ and remote sensing observations and from a recent model study. The data include ice particle concentrations, sizes, ice water content, geometrical depth, width, and optical depth. Integral properties (A_c, $N_{\rm ice}$, EA, I) are also available (Schumann et al. 2017). The observations support the assumption that the number of ice particles in contrails is controlled by the heat, humidity, and aerosol in the engine exhaust and the formation process in the jet phase, and they decrease thereafter. Artifacts produced by crystal shattering on the inlets of the particle probes can yield measurement errors, in particular when large particles are present (Korolev et al. 2011). Most contrail particles, formed at low ambient temperature, are small and, hence, shattering is likely small (Febvre et al. 2009; Voigt et al. 2011). The data synthesis shows no obvious indication, like exceptionally high ice particle concentrations, that ice particle shattering at instrument inlets had strong effects on past contrail measurements.

It is generally assumed that residuals from sublimated contrail ice particles do not get reactivated when again entering ice-supersaturated air. As noted by Zhou and Penner (2014), soot particles processed in contrails may be better ice nuclei than fresh soot. The residuals may still contain some ice in particle gaps that is not sublimated, and the residuals may be quite large when including aerosol parts from nucleation and scavenging. This topic is of relevance for both contrails and cirrus formation and has not yet been studied conclusively. If such reactivation occurs in contrails, it could explain high survival fractions of ice particles in the vortex regime.

Besides the number of ice particles, the depth D and, to minor degree, the width W of the wake vortex systems are important for the climate effect of contrails. The depth influences the optical depth (Voigt et al. 2011); W and D control volume-specific ice concentrations and D together with shear and turbulent mixing are important for subsequent horizontal spreading (Konopka 1995). The plume width during the vortex phase is close to aircraft engine span (Greene 1986) but widens during vortex breakup, for example, after vortex ring formation, and for strong stratification (Misaka et al. 2012; De Visscher et al. 2013).

A parameterization of the wake vortex descent depth D_w during the two wake vortex decay phases has been derived by Holzäpfel (2003). Recent results suggest larger descent distances than predicted. The contrail depth D_c may be smaller when the primary vortex sublimates and larger when buoyancy causes some lift above the flight level. Figure 3-4 compares results for D, that is, wake vortex depth and contrail depth, with various experimental data and LES results. The nondimensional descent D/b_0 depends on the stratification parameter $N^*_{\rm BV}$ and on turbulence ε_t^* [see Eq. (3-8)]. For low stratification, D depends strongly on ambient disturbances initiating hydrodynamic instabilities. For weak shear, vortex rings may form, after a time $6b_0/w_0$ (Delisi and Greene 2009). The results differ partly because of different initial disturbances, Reynolds number, and numerical resolution. Deep wake depths, possibly sinking beyond $D/b_0 > 20$, are observed in laboratory experiments and idealized simulations with little stratification, little turbulence, and little wind shear, and wind shear gradient (Delisi and Greene 2009). For high humidity, some of the contrail LES results show larger D. It is not clear how much the age (6 min; reaching into the dispersion phase) contributes to the larger D.

The humidity inside dense contrails decreases to ice saturation shortly after contrail formation. This is a consequence of large products $n_{\rm ice}r_{\rm area}$ (size per volume) of ice particle concentrations $n_{\rm ice}$ and ice particle sizes $r_{\rm area}$, implying small time scales $t_{\rm sat}$ of humidity relaxation to saturation by deposition–sublimation of water vapor on the ice particles, $t_{\rm sat} \approx (4\pi D_{\rm H2O} n_{\rm ice} r_{\rm area})^{-1}$ (Korolev and Mazin 2003). Here, $D_{\rm H2O}$ is the diffusion coefficient of

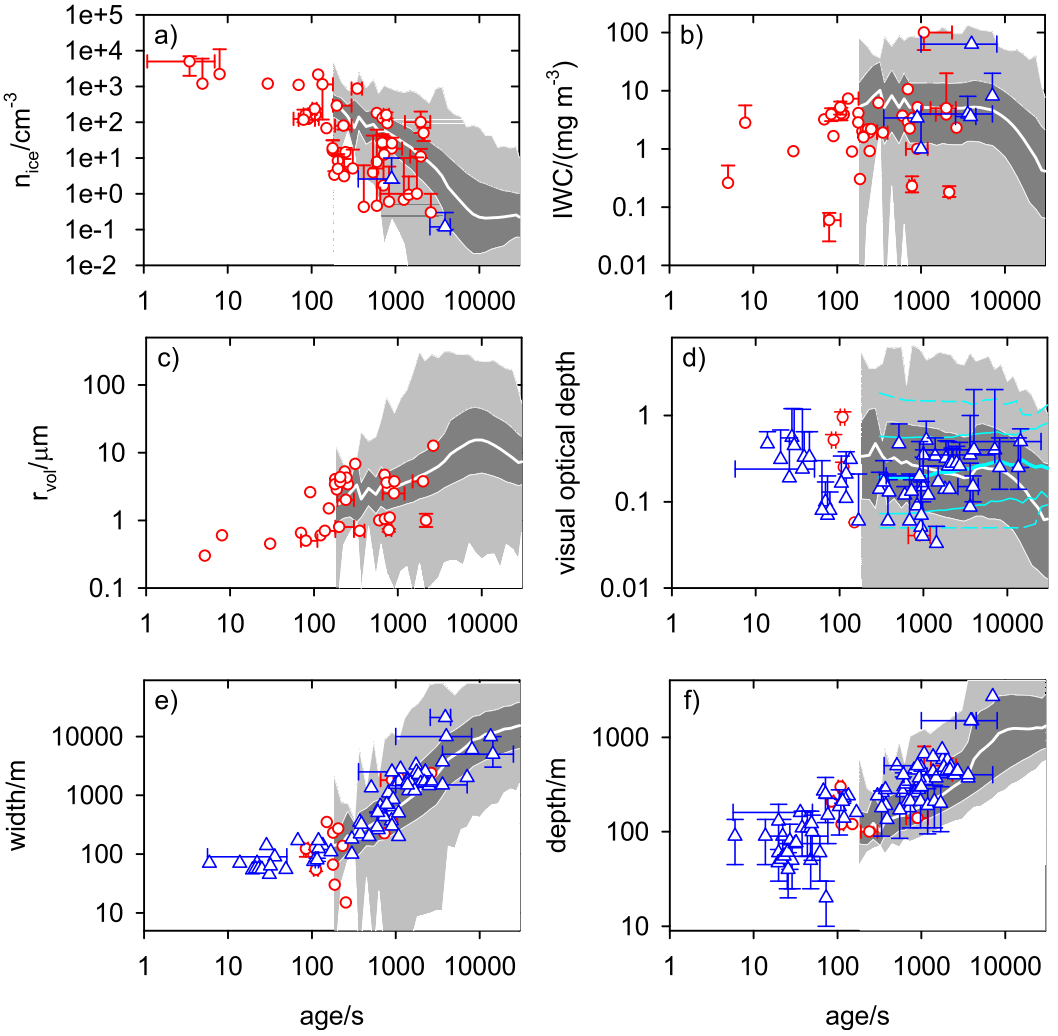

FIG. 3-3. Mean contrail properties vs age. (a) Ice number concentration, (b) IWC, (c) volume-mean radius, (d) optical depth, (e) contrail width, and (f) geometrical depth from in situ measurements (red) (Knollenberg 1972; Baumgardner and Cooper 1994; Poellot et al. 1999; Schröder et al. 2000; Gao et al. 2006; Febvre et al. 2009; Heymsfield et al. 2010; Voigt et al. 2011; Jones et al. 2012; Jeßberger et al. 2013; Schumann et al. 2013b; Kaufmann et al. 2014) and remote sensing observations (blue) (Hoshizaki et al. 1975; Baumann et al. 1993; Freudenthaler et al. 1995, 1996; Minnis et al. 1998; Spinhirne et al. 1998; Sussmann and Gierens 1999; Duda et al. 2004; Atlas et al. 2006; Atlas and Wang 2010; Schumann et al. 2013a) and from CoCiP model simulations [shaded regions with white lines for minimum, 10%, 50%, 90%, and maximum percentiles (Schumann et al. 2015)]. The cyan curves in (d) show corresponding percentiles of optical depth data from ACTA (Vázquez-Navarro et al. 2015).

water vapor in air. Kaufmann et al. (2014) measured humidity inside a contrail that was close to saturation for $n_{ice} = 117\,\text{cm}^{-3}$ and $r_{area} = 0.5\,\mu\text{m}$, implying $t_{sat} \approx 23\,\text{s}$. Here, t_{sat} is smaller than the contrail age (>90 s), in spite of the rather small ice particle sizes, in this case. Hence, RHi inside contrails is mostly well relaxed toward saturation. As visualized in LES (Naiman et al. 2011; Picot et al. 2015), deviations from saturation occur at the contrail boundaries.

The total optical extinction $\text{EA} = W\tau$ of the contrail near the end of the vortex phase depends on Q_{ext} and $N_{ice} = f_s f_c \text{PEI}_{soot} m_F$ and πr_{area}^2 [see Eq. (3-2)]. The ratio C relates r_{area}^2 with r_{vol}^2. The volume radius r_{vol}, Eq. (3-3), depends on the third root of the mean particle mass. The mean particle mass depends on the bulk density ρ_{ice} and on the amount of water per ice particle in the contrail, that is, approximately, on the water emission ($\text{EI}_{H2O} m_F$) distributed over the cross section $A_c = N_{dil} m_F/\rho$, with air density ρ, and the water uptake from ambient air, for given ice saturation pressure $p_{ice}(T)$, pressure p, temperature T, relative humidity over ice RHi, and air and water molar masses, so that (Jeßberger et al. 2013)

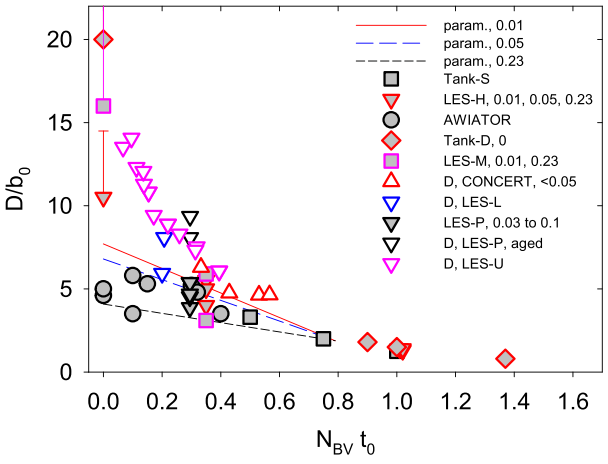

FIG. 3-4. Maximum wake vortex sinking distance or contrail depth D vs Brunt–Väisälä frequency N_{BV}, normalized with wake vortex scales. Adapted from Schumann (2012) with additions. The red, blue, and black lines depict a parameterization for fixed dissipation $\varepsilon_t^* = 0.01$, 0.05, and 0.23, respectively (Holzäpfel 2003). The value of ε_t^* is given in the legend when known. Filled symbols are for wake vortex descent from LES (Delisi and Robins 2000; Hennemann and Holzäpfel 2011; Misaka et al. 2012; De Visscher et al. 2013; Picot et al. 2015), tank experiments (Sarpkaya 1983; Delisi and Robins 2000; Delisi and Greene 2009), and field experiments [Aircraft Wing with Advanced Technology Operation (AWIATOR) project; de Bruin and Kannemans 2004]. The one-sided error bars for $N_{BV} = 0$ indicate that vortex rings may descend even further in quiet air. Open symbols are contrail depth values D from observations [CONCERT (Jeßberger et al. 2013); 1–2-min ages] and LES (Lewellen et al. 2014; Unterstrasser and Görsch 2014; Picot et al. 2015) for 4–6-min ages. Single letters in the legend identify author initials.

$$\mathrm{EA} = \left(\frac{9\pi}{16\rho_{\mathrm{ice}}^2}\right)^{1/3} C Q_{\mathrm{ext}} m_F (f_s f_c \mathrm{PEI}_{\mathrm{soot}})^{1/3} \times \left[\mathrm{EI}_{\mathrm{H2O}} + \frac{(\mathrm{RHi} - 1) N_{\mathrm{dil}} M_{\mathrm{H2O}} p_{\mathrm{ice}}(T)}{M_{\mathrm{air}} p}\right]^{2/3}. \quad (3\text{-}9)$$

Hence, EA grows linearly with fuel consumption m_F, the third root of the ice particle emission index and the ⅔ power of dilution and supersaturation.

Unexpectedly large (15–20-μm effective diameter) ice particles have been measured in young contrails during CONCERT (Jeßberger et al. 2013). The concentration of crystal with diameters exceeding 10 μm could not be reproduced with models for the measured conditions. It seems that some ice particles start to grow early (e.g., at the outer edge of the young exhaust jet, perhaps on small ambient cirrus particles), consume most of the ice supersaturation, and grow to sizes as measured, but details have not been explained.

In summary, after the wake vortex phase, the contrail contains a number $N_{\mathrm{ice}} = f_s f_c \mathrm{PEI}_{\mathrm{soot}} m_F$ of ice particles, and has depth D, width W, and an ice water content I, mainly determined by the jet and vortex dynamics, and ambient humidity, and Eq. (3-3) determines corresponding particle sizes.

e. Contrail dispersion phase

Contrails in the dispersion phase are far more difficult to explain than in the jet and wake phases. Mixing is no longer controlled by aircraft-induced motions. Instead, the atmosphere, with all its complexity, causes mixing. Initially, mixing is controlled mainly by shear and ambient turbulence. Wind shear is highly variable because of mesoscale horizontal motions. Turbulence at flight levels is difficult to predict for many reasons (Sharman et al. 2012; Paoli et al. 2014). Latent heat effects are small for low temperatures. However, radiative heating can contribute to destabilize the cirrus and contrail layers by infrared cooling at cloud tops and terrestrial warming from below, in addition to heating by absorption of solar radiation (Jensen et al. 1998a; Unterstrasser and Gierens 2010b). The process gets far more complex when ice sedimentation gets important, and contrail particles fall into drier or more humid air below the contrail levels (Bock and Burkhardt 2016a). The terminal fall speed of particles depends on their size (Reynolds number) and habit (Heymsfield et al. 2013). By sedimentation, large particles separate from the smaller ones, thinning the upper contrail part. The upper part contains most of the exhaust and may still contain a considerable number of small particles, observable as the "contrail core." Smaller ice particles may sublimate earlier than larger ones, in particular when the Kelvin effect becomes important, causing in situ particle losses (Lewellen et al. 2014). Falling ice particles may aggregate with smaller ice particles causing a reduction of the number of ice particles (Kienast-Sjögren et al. 2013). When the larger particles fall into more humid air, the ice particles grow and fall even more quickly, so that fall streaks develop and eventually precipitate (Freudenthaler et al. 1995; Atlas et al. 2006; Unterstrasser et al. 2012). Hence, the thickness D_{IS} of the ice-supersaturated layer below the contrail influences the life cycle (Sussmann and Gierens 1999; Lewellen 2014). Finally, one has to consider cirrus–contrail interactions. Contrail and natural cirrus particles, when present, compete for ice-supersaturated air, and this may have strong effects for growth of existing ice particles and nucleation of additional ice particles. Little is known about potential new contrail ice particle formation during the contrail life cycle. However, the observations collected in Fig. 3-3 support the assumption that the number of ice particles in contrails does not increase with contrail age (Spinhirne et al. 1998).

The period of contrail existence of radiative importance may be shorter than the whole lifetime: The region in which contrails form may get covered by natural cirrus after contrail formation. Contrails sedimenting into other clouds may get radiatively shielded by the clouds above the contrail.

One may distinguish between externally and internally limited life cycles of contrails. Contrails are considered to be limited externally when the changing meteorology limits the lifetime, for example, by sublimation in subsiding air masses. Contrails are limited internally, when the contrails end by sublimation or sedimentation even for fixed meteorology. For both kinds of contrail cirrus, the energy forcing EF [time integral of local radiative forcing RF′ weighted with contrail width (Schumann et al. 2012a)] depends on the lifetime. To first order, the EF of externally limited contrails increases with the square of the lifetime and the third root of the number of contrail ice particles per flight distance. For internally limited contrails, the EF depends even more strongly on N_{ice}.

The ice mass I and optical depth τ of contrails increases as RHi increases (Unterstrasser and Gierens 2010a). But this does not necessarily imply that high RHi gives a high climate impact EF. Contrail particles remain small for low ice supersaturation but may exist for a long time because of low fall speeds. For high humidity, the contrail ice particles get large but sediment quickly, so that EF may get largest for weak but long lasting supersaturation (Lewellen 2014; Schumann et al. 2015).

In situ measurements of aged contrails are difficult because the pilots can hardly distinguish aged contrails from thin cirrus during flight. Thick contrails were followed for ages up to 40 min (Heymsfield et al. 1998; Schröder et al. 2000; Febvre et al. 2009; Jones et al. 2012) and results are included in Fig. 3-3. Many aged contrails have been sampled with novel cloud instruments on the new High Altitude and Long Range Research Aircraft (HALO) during the Midlatitude Cirrus Experiment (ML-CIRRUS) campaign in 2014 (Voigt et al. 2016). In fact, natural cirrus, totally unaffected by aircraft emissions, is rare over Europe. Contrails were measured for contrail ages of at least 1.8 h. Contrail cores were identified from enhanced NOx emissions, traffic data, and trajectory analysis. These contrail parts were found to have still higher concentrations of relatively small ice particles than ambient cirrus.

Important progress has also been achieved by remote sensing of contrails. More than 3400 contrails have been identified in collocated MODIS–*CALIPSO* images (Iwabuchi et al. 2012). The data brought important statistics on contrail occurrence in the Northern Hemisphere and on altitude, width, depth, and length of contrails; lidar backscatter and depolarization; and optical depth. The thinnest contrails detectable in this manner have optical depth >0.03.

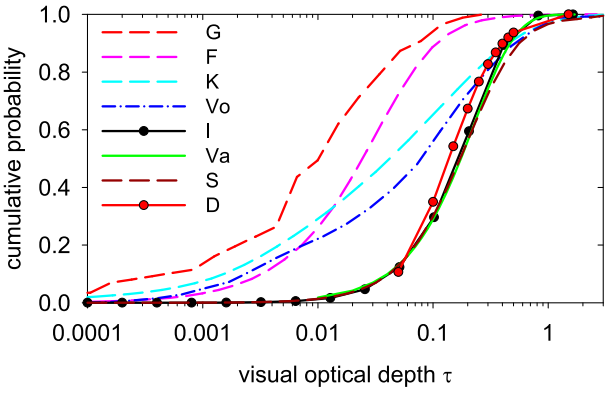

FIG. 3-5. Cumulative probability distribution of optical depth of contrail cirrus from simulations and observations. Adapted from Grewe et al. (2014b) with additions. G: Grewe et al. (2014b); F: Frömming et al. (2011); K: Kärcher and Burkhardt (2013); Vo: Voigt et al. (2011); I: Iwabuchi et al. (2012); Va: Vázquez-Navarro et al. (2015); S: Schumann et al. (2015); D: Duda et al. (2015).

Contrails were identified from MODIS and Meteosat satellite images with an automatic contrail detection algorithm (ACTA) and traced forward and backward in time in Meteosat images with 5-min temporal and ~4-km horizontal resolution (Vázquez-Navarro et al. 2015). The study observed 2400 contrails, mainly over the Atlantic and Europe at northern midlatitudes, partly multiple times (with increasing ages) during their life cycle up to maximum ages (lifetimes) of 19 h, and evaluated their optical depth (see Fig. 3-5), height, width, shortwave (SW) and longwave (LW) RF′, as induced by contrails visible, after some dwell time, to Meteosat. Figure 3-6 depicts the observed ages of contrails detected this way. Mean values retrieved are 1 h in age, 130 km in length, 8 km in width, 11.7 km in altitude, and 0.34 in optical thickness. Local RF′ values of order $\pm 20\,W\,m^{-2}$ and EF values of up to $400\,GJ\,km^{-1}$ during night and $-875\,GJ\,km^{-1}$ over water during daytime were derived. Many contrails are cooling during day. Figure 3-7 compares the local RF′ values derived from these data with results computed with the Contrail Cirrus Prediction Model (CoCiP) coupled to the climate–aerosol model Community Atmosphere Model—Integrated Massively Parallel Atmospheric Chemical Transport (CAM3+/IMPACT; Schumann et al. 2015). The model computes thick and thin contrails with small RF′ values, while the observations see mainly the thicker contrails. Both show positive LW and negative SW local RF′ values of order $20\,W\,m^{-2}$, about 1000 times larger than the global mean, consistent with previous observations (Khvorostyanov and Sassen 1998; Haywood et al. 2009; Laken et al. 2012).

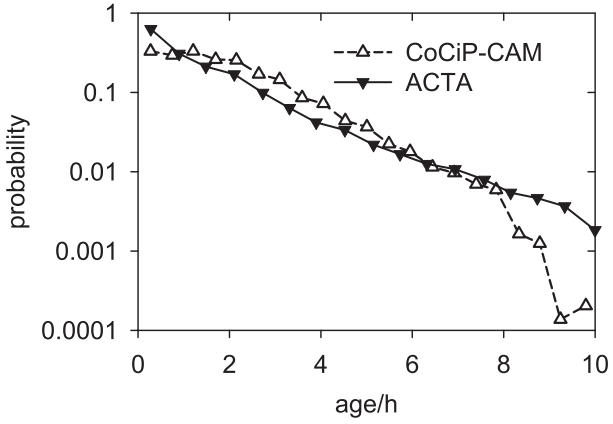

FIG. 3-6. Probability density functions of ages of contrails in simulations (CoCiP–CAM) and in satellite observations (ACTA). Data from Schumann et al. (2015) and Vázquez-Navarro et al. (2015).

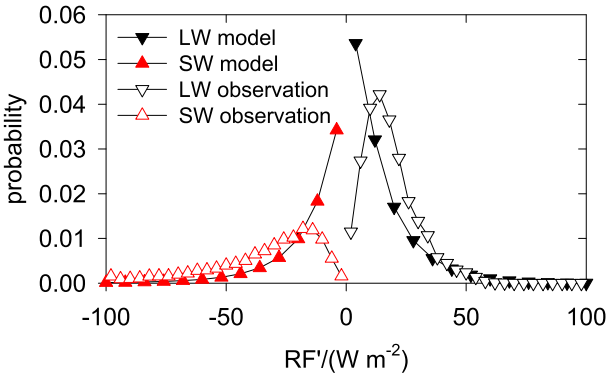

FIG. 3-7. Probability density functions of local LW (black) and SW (red) RF′ of contrails derived from satellite observations (open symbols; ACTA; Vázquez-Navarro et al. 2015) and a coupled contrail–climate model simulation (closed symbols; Schumann et al. 2015).

Much has been learned about the fate of aged contrails during dispersion using LES models. Lewellen (2014) analyzed lifetime-integrated properties from 200 individual contrail LES simulations. Contrails reached lifetimes > 40 h, widths > 100 km, and ice masses $> 50\,\mathrm{kg\,m^{-1}}$. The lifetime-integrated ice crystal surface area per length of flight path $\mathrm{SS} \sim \int N_{\mathrm{ice}} \pi r_{\mathrm{area}}^2 \, dt$ is used as an approximate metric of contrail climate significance. For constant radiative properties of the ice particles, this integral is related to the energy forcing discussed before. Over much of the parameter space, SS is found to vary approximately with the product of the maximum contrail depth and effective number of ice crystals per flight path. None of the LES studies includes the full variability of ambient meteorology, so lifetimes are likely overestimated.

The scale range from single-engine jets to the global scale is too large to be covered by LES. Hence, simplified models are used to bridge the scales. Simplified models may be based on scale analysis (Lewellen 2014). An alternative is to use a Lagrangian contrail model, which follows individual contrail segments, using data from weather predictions or climate models, and to simulate the life cycle of all individual contrail segments as forming for given traffic routes from the global fleet of aircraft. Such an approach has been implemented in CoCiP (Schumann 2012). As shown in Figs. 3-3–3-7, the range of model results is in general agreement with the available observations.

f. Optical properties

The climate impact of contrails depends on the optical properties of ice particles and contrails, that is, besides size and number, mainly on particle habit and contrail optical depth (Yang et al. 2015). Ice particles are never exactly spherical but may have a near-spherical shape (possibly droxtals; Thuman and Robinson 1954) just after freezing from liquid droplets, and become more nonspherical in humid air quickly thereafter (Bailey and Hallett 2009). Nonspherical ice particles backscatter solar light more strongly laterally and backward than do ice spheres. Ice particles with rough surfaces may scatter more strongly than with smooth surfaces. Hence, the SW RF by contrails is underestimated (the net RF is overestimated) when spherical ice crystals are used to represent contrails (Meerkötter et al. 1999; Markowicz and Witek 2011). Schröder et al. (2000) found near-spherical ice particles of a few microns in size in young contrails and nonspherical ones in aged contrails and in thin cirrus from images of replica on coated films. Jones et al. (2012) found small ($\approx 10\,\mu$m) platelike crystals in persistent contrails, while larger particles retained a hexagonal habit. Hexagonal plates were also deduced from optical halo observations in aged contrails (aufm Kampe 1943; Sussmann 1997). Gayet et al. (2012) found a decrease of the asymmetry parameter of contrail particles with contrail age in the wake of an A380 aircraft until 4 min of contrail age. Xie et al. (2012) derived a contrail habit parameterization matching lidar-observed contrails (Iwabuchi et al. 2012). Schumann et al. (2011) suggested a size-dependent particle habit mix for contrail cirrus studies by combining droxtal-shape particles for small contrail particles and a parameterization for cirrus (Baum et al. 2005) for large contrail particles.

The cumulative distribution function of optical depth τ (near 550 nm) has a negative skewness (see Fig. 3-5): A few contrails get thick while most have small τ; some are subvisible, and only the thicker ones are observable (Immler et al. 2008; Kärcher and Burkhardt 2013). Early studies assumed large τ values, based on a few lidar

observations (Meerkötter et al. 1999). Some global models suggest large fractions of subvisible contrails and τ mean values of about 0.05 (Ponater et al. 2002; Grewe et al. 2014b). The optical depth of contrails is often large for young contrails because of many ice particles of sufficient size, grown by uptake of ambient humidity in narrow plumes with large depths (Freudenthaler et al. 1996; Voigt et al. 2011). Later, τ may grow in rising air masses with increasing humidity but generally decreases and approaches zero while the contrails spread laterally and finally sublimate. Ground-based lidar and camera observations (Atlas and Wang 2010) detected 200 thin contrails (average optical depth of 0.2) but one exceptionally thick contrail ($\tau \approx 2.3$) under very humid conditions. A collection of observed τ data is included in Fig. 3-3. Contrail cirrus may have 2–3 times larger optical depth than derived for linear contrails (Bedka et al. 2013; Minnis et al. 2013). A global mean optical depth $\tau \approx 0.29$ of contrail cirrus was computed in a global model (Schumann et al. 2015). The relatively thick contrails detected with MODIS–CALIOP (Iwabuchi et al. 2012) and with ACTA from Meteosat observations (Vázquez-Navarro et al. 2015) have similar optical thickness, with a mean of 0.25–0.35. Hence, the mean optical depth of aged contrails is likely larger than estimated some years ago.

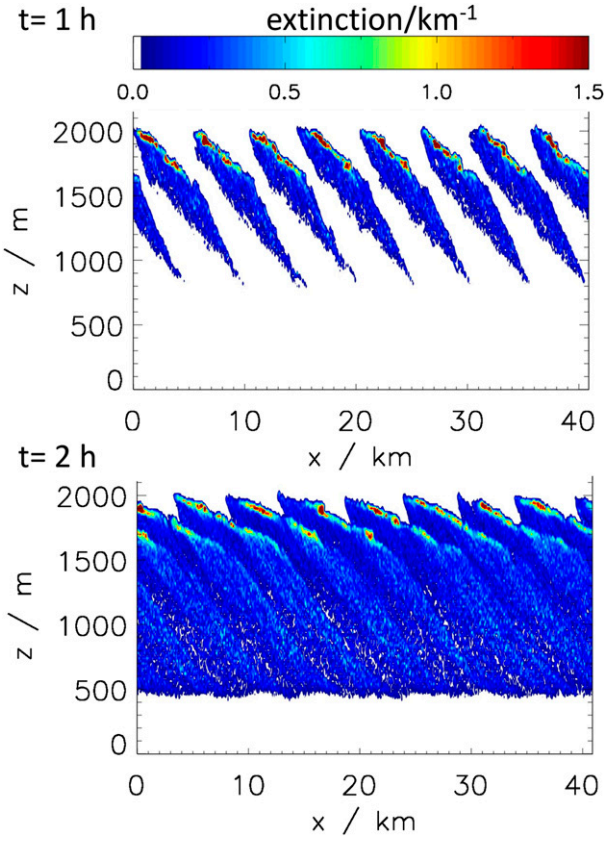

FIG. 3-8. The development of the extinction of a contrail cluster consisting initially of 8 individual contrails with time: (top) 1 h; (bottom) 2 h. Adapted from Unterstrasser and Sölch (2012).

3. Contrail cirrus

a. Transition of contrails into contrail cirrus

Eventually, contrails change their morphology depending on the humidity, shear, stratification, waves, turbulence, radiative heating, etc. Individual contrails mix with other contrails and with other cirrus (see Fig. 3-1g), forming ''contrail cirrus'' (Liou et al. 1990; Schumann and Wendling 1990). Overlapping contrails produce less total extinction than individual contrails, because of competition for humidity. This competition is nicely illustrated in Fig. 3-8. Hence, the climate impact increases less than linearly with traffic density (Unterstrasser and Sölch 2012). The transition of an individual contrail into contrail cirrus can be observed for an aircraft flying spirals, as shown for an impressive example in Fig. 3-9 (Haywood et al. 2009). ''Contrail outbreaks'' contain many aged and young contrails simultaneously and spread over large areas (Duda et al. 2001).

b. Meteorological conditions for contrail occurrence

Contrail assessments require accurate data on ambient meteorology. The SAC criterion for contrail formation is satisfied only at low enough temperatures. Contrail persistence depends on a humidity threshold. Relative humidity depends on saturation pressure and hence on temperature, and temperature and vertical motions are key determinants for humidity. Also the optical properties and life cycle of contrails depend strongly on meteorological properties, in particular on wind shear, vertical motions, turbulence, and ambient cirrus clouds. Even more important, the RF and climate impact depend on all these meteorological parameters and in addition on the albedo and the brightness temperature of the atmosphere without contrails (Schumann et al. 2012a).

Great progress has been achieved in numerical weather prediction (NWP) models with proper data assimilation over recent decades (Bauer et al. 2015). Hence, one may assume that temperature can be well predicted. In fact, NWP data have been found to differ from in situ data at flight levels by less than 0.5 K on average (Dyroff et al. 2015). Such accuracies are more difficult to achieve in climate models, without data assimilation, which often suffer from a cold temperature bias at the tropopause (Marquart et al. 2003; Irvine and

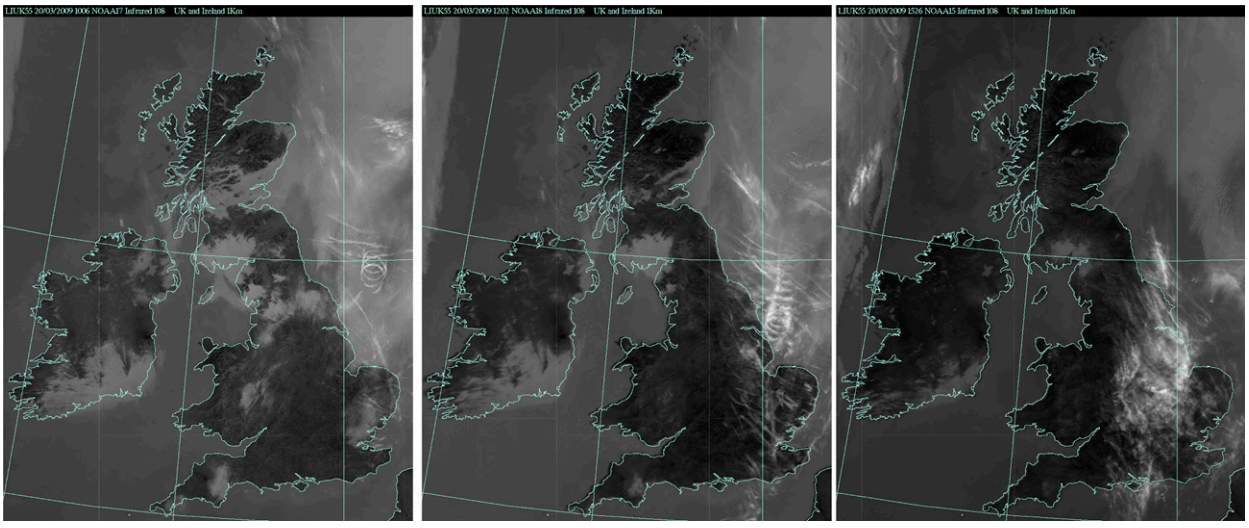

FIG. 3-9. Evolution of contrail cirrus from a spiral flight. Contrail cirrus is identified by bright white areas with low infrared (10.8 μm) brightness temperature. The satellite scenes are from NOAA AVHRR for 3 UTC times: (left) 1006 (age ≈ 1 h), (center) 1202 (age ≈ 3 h), (right) 1526 (age ≈ 6.5 h). Adapted from Haywood et al. (2009).

Shine 2015; Wu and Pauluis 2015). A cold bias not only increases the apparent relative humidity and the frequency of contrail formation but also increases the computed LW RF of contrails at those temperatures.

Until recently, there was some uncertainty whether persistent contrails form only in cloud-free supersaturated areas or also inside cirrus (Spichtinger et al. 2005; Burkhardt et al. 2008). Contrail formation in clear sky can be observed often. But contrails also form when the sky is covered, possibly with thin or even subvisible cirrus (Immler et al. 2008). The SAC threshold temperature of contrail formation is slightly higher in cirrus than in clear air (Gierens 2012), because the IWC from cirrus adds some humidity. High ice supersaturation has been measured in situ outside and inside cirrus (Ovarlez et al. 2000; Jensen et al. 2001; Ovarlez et al. 2002; Comstock et al. 2004). Ice saturation inside cirrus is to be expected for long time scales of return to saturation, that is, for small mean sizes of ice particles per volume (product $r_{\text{area}} n_{\text{ice}}$; Korolev and Mazin 2003). Contrails embedded in cirrus have been observed and are not much thinner than clear-air contrails (Gayet et al. 1996; Poellot et al. 1999).

The frequency of ice-supersaturated regions (ISSR) in the upper troposphere is not reliably known. Figure 3-10 compares mean frequencies of ice supersaturation from a global climatology of ISSR inferred from satellite data, NWP results, and a climate model with thin-cloud frequencies from a spaceborne lidar (Lamquin et al. 2012). Climate models tend to overestimate mean ISSR occurrence above the tropopause. Local ISSR are generally shallow, located close to the tropopause with sharp temperature changes (Birner et al. 2002), and form preferably in regions with upwind and divergent airflow (Gierens and Brinkop 2012). ECMWF interim reanalysis (ERA-Interim) data imply a mean frequency of 10% of ISSR at 250 hPa (Irvine and Shine 2015). Airliners fly possibly 15% of their time in ice-supersaturated air masses (Gierens et al. 2012), with a mean length of about 150 ± 250 km (Gierens and Spichtinger 2000) that is seasonally variable (Spichtinger and Leschner 2016), consistent with observed contrail occurrences and lengths (Minnis et al. 2003; Iwabuchi et al. 2012). The layers are often 600–800 m thick (extreme values 25–3000 m), with 30% less than 100 m (Dickson et al. 2010).

So far, most NWP use one-moment prognostic cloud schemes (only ice mass, not ice number). Some climate models use diagnostic parameterization with assumptions on subgrid-scale humidity variability (Burkhardt et al. 2008). Several recent models permit ice supersaturation to occur (Liu et al. 2007; Lohmann et al. 2008), at least in the clear-sky portion of a grid cell (Tompkins et al. 2007). Irvine and Shine (2015) analyzed data from five models used for climate assessments and found that the frequency of exceeding 90% humidity in the annual and global mean at 250 hPa varies from 1% to 19% (compared to 11% for ERA-Interim).

Accurate routine measurements of humidity values at tropopause levels are demanding. The recently revised MOZAIC dataset (Smit et al. 2014) may be used to test previous estimates on ice supersaturation occurrence. Relative humidity depends on saturation conditions; a 0.5-K temperature bias causes 7% change in RHi at

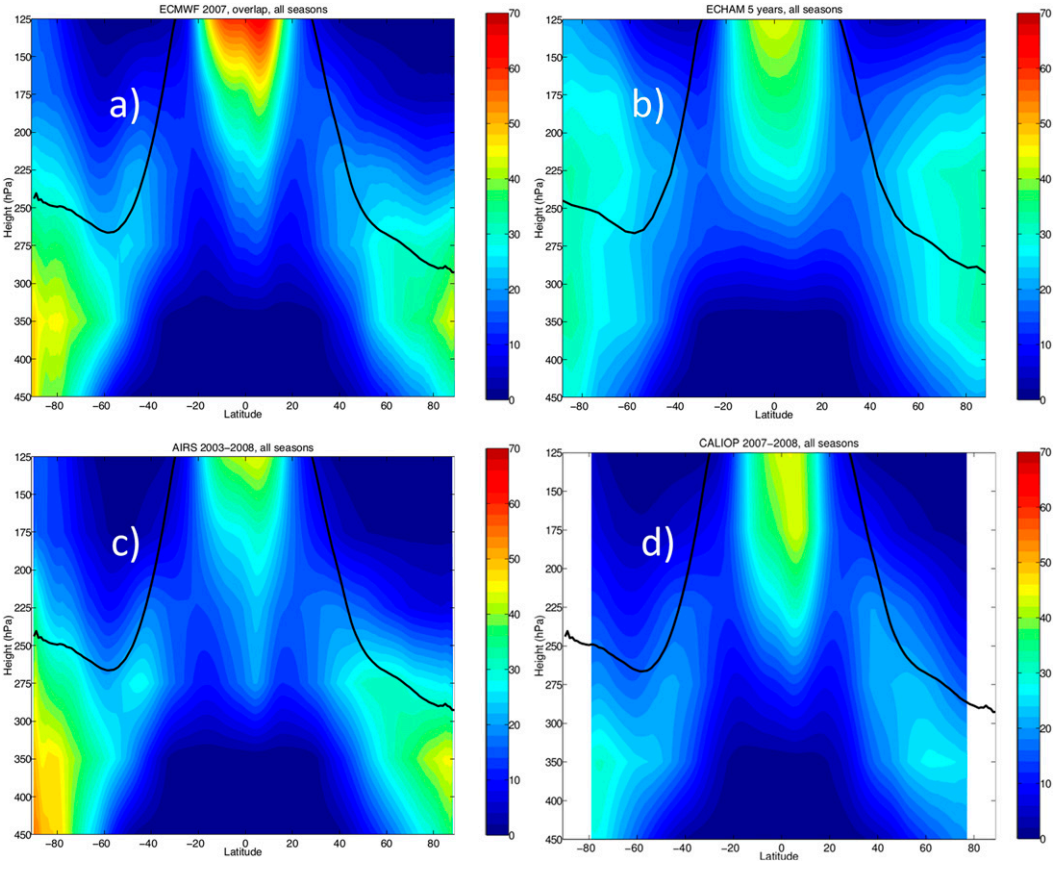

FIG. 3-10. Zonal means of ice supersaturation occurrence frequencies (%) from (a) ECMWF, (b) ECHAM, and (c) AIRS, and (d) frequency of high cloud occurrence from CALIOP. The lines depict the zonal mean tropopause, as computed from the AIRS data, in all panels. Adapted from Lamquin et al. (2012).

temperature of −60°C. Aircraft humidity measurements have to be corrected for adiabatic heating by air compression in inlets, by 30 K for 240 m s^{-1} speed, in addition to sensor deicing heating (Helten et al. 1999). An RHi accuracy of 10% is not easy to reach, therefore. During research measurement with the German Aerospace Center [Deutsches Zentrum für Luft- und Raumfahrt (DLR)] Falcon, the sensors often indicated a slightly subsaturated ambient humidity (RHi = 95%) while the contrail that was measured was clearly increasing in IWC to amounts that could be explained only if RHi was near 115% (Gayet et al. 2012; Jeßberger et al. 2013).

c. *Contrail coverage*

Contrail coverage is ill defined for several reasons. The product of contrail coverage and optical depth controls the RF (Lee et al. 2010). For a single contrail segment, this product equals the total extinction, EA. However, difficulties arise when coverage is diagnosed independently of optical depth. Young contrails are distinguished from other cirrus based on their line shape, and this criterion gets uncertain when the contrail gets deformed (Mannstein et al. 1999). Only a small fraction of all linear contrails are detectable from satellites (Mannstein et al. 2010; Minnis et al. 2013). The global contrail coverage was estimated in early studies from regional satellite observations, a potential contrail coverage for given temperature and humidity data, and traffic density (Sausen et al. 1998). Hemispheric observations became available only recently (Duda et al. 2013). Hence, it is not surprising that the coverage of line-shaped contrails derived from satellite data and models varies from about 0.06% to 0.15% (Rap et al. 2010b; Frömming et al. 2011; Duda et al. 2013). The coverage by contrail cirrus may be far higher than by line-shaped contrails, and factors of order 10 (Minnis et al. 2004; Stordal et al. 2005; Burkhardt and Kärcher 2011; Graf et al. 2012) have been reported; but there is no unique ratio because it depends on the detectability of both the line-shaped contrails and the total contrail cirrus.

Burkhardt and Kärcher (2011) quantified the amount of contrail cirrus using the ECHAM contrail cirrus global climate model (CCmod), which includes a subgrid-scale cloud class of young contrails. The model captures the life cycle of these man-made clouds and simulates their global coverage as well as the changes in natural cloudiness that they induce. They computed contrail cirrus coverage of about 0.23%. Recent attempts to quantify contrail cirrus from MODIS data, allowing for more diffuse contrail contributions, resulted in similar global coverage (Minnis et al. 2013). In CoCiP, the global contrail coverage is computed by superposing the τ contributions from all individual contrails and ambient cirrus and counting fractions of areas in which contrails cause the optical depth of the total cirrus to exceed a certain threshold (Schumann 2012). Contrails not only enhance cloud coverage but also thicken existing cirrus (Minnis et al. 2013; Schumann and Graf 2013) by causing more ice particles, with smaller effective radius, at constant ice water content (Kristensson et al. 2000). This does not exclude that contrails consume humidity and hence reduce natural cirrus (Burkhardt and Kärcher 2011; Unterstrasser and Görsch 2014; Schumann et al. 2015), but the thickening by many additional small ice crystals seems to dominate.

d. Contrail–cirrus–soot interactions

Soot from aviation may change cirrus properties also without prior contrail processing, causing ''soot cirrus'' (Jensen and Toon 1997; Penner et al. 2009; Lee et al. 2010). Modeling studies of the climate impact of aviation soot cirrus remain inconclusive because of the uncertainties in soot abundance and ice-nucleating properties (Koehler et al. 2009; Hendricks et al. 2011; Gettelman and Chen 2013; Zhou and Penner 2014). Enhanced small-sized cirrus particle concentrations with patterns similar to aviation-soot emissions (Ström and Ohlsson 1998; Kristensson et al. 2000) have been observed by in situ measurements in cirrus in regions with dense air traffic. It is open whether the soot entered the ice during nucleation or later by scavenging.

From sublimation of cirrus particles that contain soot (and sulfate) from nucleation or scavenging, soot aggregates may form, possibly with some acid water remainders, which may act as efficient ice nuclei later. On 3 November 2012, a special cirrus pattern was observed near Munich, Germany, as documented with several cameras and ground-based lidar and radar. The camera observation method is described in Schumann et al. (2013a). The cirrus was observed between 9.1- and 9.5-km height, was 8–10 km wide, and 35–50 km long. The ambient temperature was below −42°C and the air was ice supersaturated. The cirrus cloud showed a pattern of cirrus with up to 10 parallel line clouds, as if it was formed from aged soot plumes (see Fig. 3-1e). Back trajectories show that soot was emitted upstream about 12 h before the event by aircraft. The air ascended and formed cirrus about 4 h before the event. The cirrus lasted for about 1–2 h and then subsided some time and sublimated. About 40 min before the event, the air ascended again and formed the observed cirrus patch. Hence this could be cirrus formed on preactivated aircraft soot. Unfortunately, it cannot be excluded that the same pattern would have formed without air traffic.

e. Contrail radiative forcing and efficacy

The RF of contrails is the change in net radiances at top of the atmosphere (TOA) for adding contrails to a given atmosphere (Fuglestvedt et al. 2010). A positive RF causes a mean warming of the atmosphere. A recent study (Dietmüller et al. 2016) confirms that the instantaneous RF does not differ much from the adjusted RF, which is used as global metric for climate change (Penner et al. 1999). In contrast, RF′, the local RF can be defined as the instantaneous change in net incoming radiation for 100% contrail coverage locally. Contrail RF is composed of a LW part and a SW part, which depend on traffic and time of day (see Fig. 3-11). In addition, RF depends on several contrail and Earth–atmosphere system parameters (Meerkötter et al. 1999). Foremost, RF′ of a contrail cirrus layer depends on the optical depth τ (at solar wavelengths), $\mathrm{RF}' \approx (d\mathrm{RF}'/d\tau)\tau$, where the change of RF′ with optical depth is of order 100 W m^{-2}. The dependency of RF on IWP is less systematic than on τ (De Leon et al. 2012; Schumann et al. 2012b). The LW RF is positive day and night, and largest for a cold contrail (near the tropopause) over a warm cloud-free Earth surface. The shortwave RF is mostly negative and largest for contrails over dark surfaces (e.g., cloud-free oceans; Meerkötter et al. 1999). A new parameterized model was developed to compute the contrail RF (Schumann et al. 2012b) for millions of contrail segments efficiently. The model calculates the RF using the TOA radiances for the contrail free atmosphere as input, as available from NWP. The model parameters are fit to accurate calculations with libRadtran (Mayer and Kylling 2005) over a range of conditions. The model and observations show large regional RF′ values (see Fig. 3-7).

The contrail RF computed within a global model depends on the representation of the contrails, on the state of the atmosphere, and on the radiation transfer model used. Myhre et al. (2009) defined a useful test of contrail RF computations, also applied by others (Rap et al. 2010b; Frömming et al. 2011; Schumann et al. 2012b; Grewe et al. 2014b; Dietmüller et al. 2016). The test

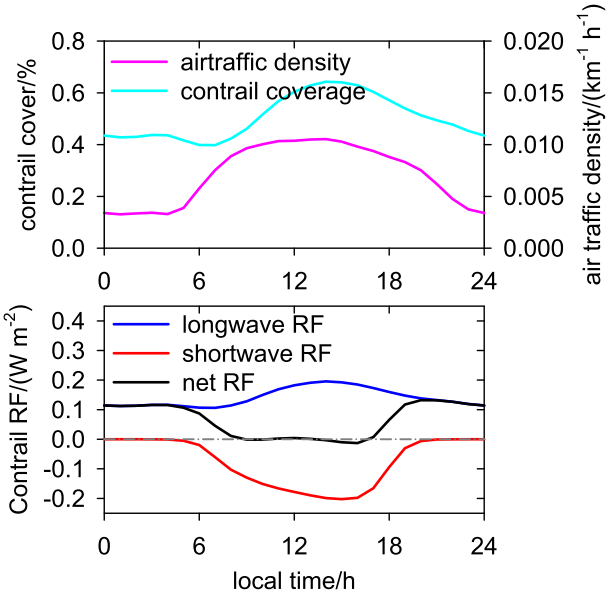

FIG. 3-11. Global mean diurnal cycle of (top) air traffic density, contrail cirrus coverage, and (bottom) LW, SW, and net RF vs local time, as derived from model simulation results (Schumann et al. 2015).

considers a 1% homogeneous contrail coverage with fixed contrail properties around 10.5-km altitude and optical depth of 0.3. For various atmosphere and radiation transfer models, the comparison revealed net contrail RF values ranging within a factor of 2. However, the results vary far more when each model uses its own selection of optical contrail properties. Unfortunately, the papers reporting results on the Myhre test so far failed to document the contrail temperature, Earth albedo, etc., which would be needed to explain RF model differences. The ratio of the absolute values of the SW RF to LW RF varies in these and other studies from 0.2 to 1 (Schumann and Graf 2013). The net RF depends on how far the LW and SW components cancel each other. For fixed LW RF, the net RF is the smaller the larger the absolute SW/LW RF ratio. This uncertainty is of great importance for quantifying contrail net RF (Boucher et al. 2013). Combined observational and model studies are needed to constrain the SW/LW RF ratio better for contrails and cirrus.

The RF by contrails has been computed in a variety of model studies. Burkhardt and Kärcher (2011) compute an RF due to contrail cirrus of about 31 mW m^{-2}, including -7 mW m^{-2} for reduced natural cirrus because the contrails consume part of the available water. For slightly higher traffic density (year 2006 instead of 2002), a revised version of this model computes a total contrail cirrus RF of 56 mW m^{-2} (Bock and Burkhardt 2016b). Chen and Gettelman (2013) compute smaller contrail cirrus RF values, 13 ± 10 mW m^{-2}. Their model assumes far smaller contrail cirrus ages and ice water

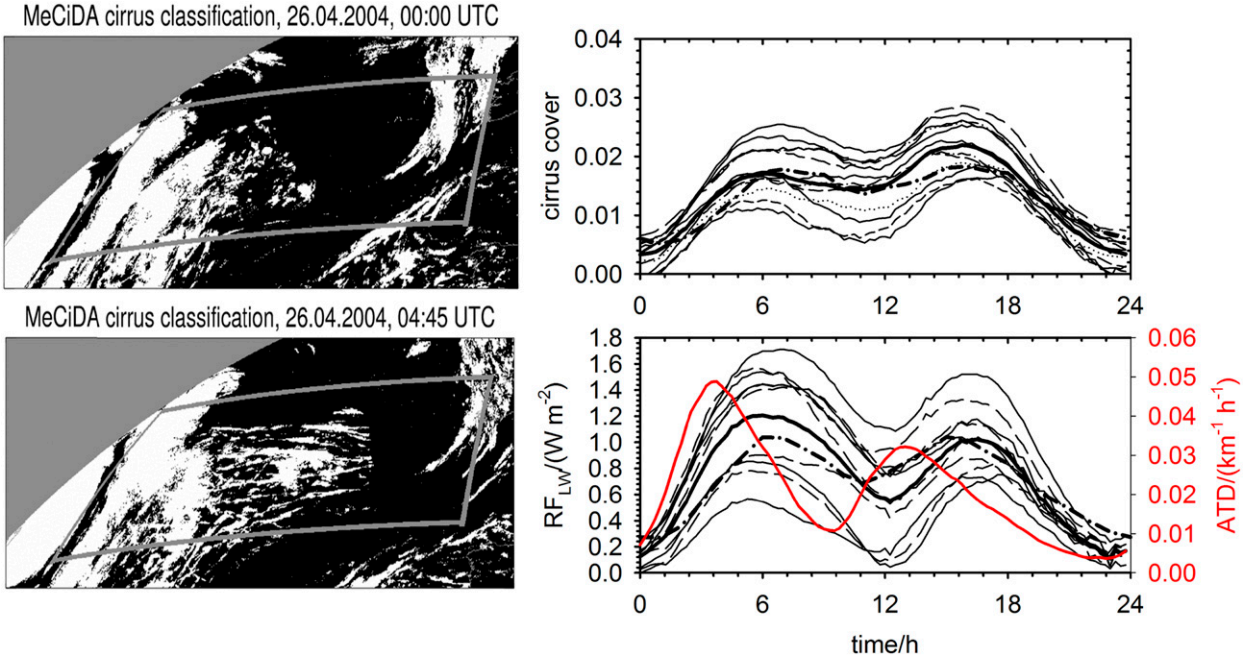

FIG. 3-12. (left) Cirrus coverage (for $\tau > 0.1$) in a North Atlantic region, shortly (top) before (0000 UTC) and (bottom) after (0445 UTC) passage of a large number of airliners from North America to Europe (Graf et al. 2012). (right) Diurnal cycle of (top) cirrus coverage and (bottom) LW RF in the North Atlantic region vs time of day as derived from Meteosat observations, for 8 individual years (thin lines) and in the 8-yr mean (thick lines), and as modeled with CoCiP (thick dashed–dotted). The red line shows the diurnal cycle of air traffic density (ATD). Adapted from Schumann and Graf (2013).

contents than other models. Schumann and Graf (2013) determined the RF from aviation-induced cloud changes (beyond individual contrails) by combining observations and model results (see Fig. 3-12). A double peak in the diurnal cycle of cirrus coverage and outgoing LW radiation was detected in the North Atlantic region in correlation with air traffic peaks: one in early morning and one during afternoon. Single images of cirrus derived from Meteosat with the MeCiDa algorithm (Ewald et al. 2013) often show cirrus patterns indicating aviation-induced cirrus changes [for an animation see Graf et al. (2012)]. The mean change in outgoing longwave radiation derived from the observations amounts to 600–900 mW m^{-2} for the North Atlantic, a large regional value. CoCiP simulates similar diurnal cycle results for given traffic and meteorological data from ECMWF, but only when increasing humidity by about 10% in the upper troposphere. Extrapolation with global/regional RF ratios from several models implies a global net RF of about 50 mW m^{-2} (40–80 mW m^{-2}; Schumann and Graf 2013). These results were used to assess the mean RF and its uncertainty range (IPCC 2013). Recently, CoCiP was run coupled with CAM3+/IMPACT to study the effects of humidity exchanges between contrails and cirrus and the redistribution of humidity in the atmosphere by contrail ice particles (Schumann et al. 2015). The RF values from some of these studies are compiled in Fig. 3-13. The net RF results differ less between the simulations than the SW to LW ratio. In all these results, the net RF is positive (implying warming) in the global mean, with an important diurnal cycle. Still, individual contrails often cool, and the local RF′ values are far larger than the global mean values (Fig. 3-7).

The global net RF is often taken as a first-order estimate of the global-mean surface temperature change ΔT_s (Fuglestvedt et al. 2010), $\Delta T_s = \lambda \mathrm{RF}$, with a climate sensitivity parameter λ of 0.8 ± 0.4 K W^{-1} m^2 for a doubling of CO_2 (Stuber et al. 2005). Different forcing mechanisms can have very different λ. The ratio of λ for contrail-cirrus RF to that for RF from CO_2 is the "climate efficacy" (Hansen et al. 2005) of contrail cirrus. The efficacy of contrail RF is not well known. Reported efficacy values vary from 0.3 (Rap et al. 2010a) to 0.6 (Ponater et al. 2005). The LW RF and the SW RF of contrail cirrus

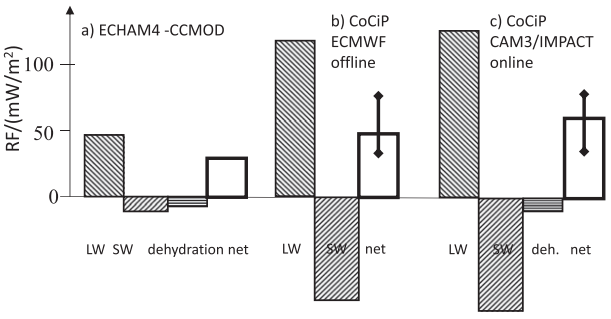

FIG. 3-13. Global mean RF from contrail cirrus [dehydration (deh.): from humidity changes in the background atmosphere; net: sum]. Results from three global model studies: (a) Burkhardt and Kärcher (2011), (b) Schumann and Graf (2013), and (c) Schumann et al. (2015).

follow from different forcing mechanisms (LW warming in the upper troposphere, SW cooling at the surface, different diurnal cycles). It may turn out that the warming by contrails is far less than what the RF suggests.

4. Achievements, open issues, and the way forward

Since recent reviews (Heymsfield et al. 2010; Lee et al. 2010), much progress has been made in understanding contrail formation and contrail cirrus: Recent studies cover the whole life cycle of contrails. The coupling of contrail formation processes with other climate system components has been modeled to some degree. Some first observational constraints for contrail cirrus occurrence and RF have been developed. Key parameters controlling the climate impact of contrails have been identified, as summarized in Table 3-1. Observation data of contrail properties compare reasonably with model results. No obvious indication for strong shattering effects has been found in past contrail measurements.

Several open issues limit progress: It is unclear why contrails are often optically thicker than expected from measured or modeled humidity. Is this an effect of underestimated ice supersaturation, small-scale vertical motions causing locally higher humidity, or additional particle production? The global climate impact of contrails depends strongly on the SW/LW RF ratio. Is the uncertainty a consequence of the habit and optical properties of the ice particles or of ambient temperature

TABLE 3-1. Key parameters controlling contrail properties and effects.

Number of ice particles in young contrails, N_{ice}	Contrail lifetime, age	Climate impact
Emissions, wake dynamics	Initial number of ice particles	Total extinction and lifetime
Number of soot particles	Ambient RHi, T, p, D_{IS}	Temp
Ambient RHi, p, temp	Mixing and sedimentation	Solar and terrestrial top of the atmosphere radiances
Particle losses in sinking wake vortex	Ambient vertical motion	Efficacy

TABLE 3-A1. List of symbols.

Symbol	Description	Unit
A_i, A_c	Area of an ice particle and contrail cross section	m^2
b_0	Wake vortex scale	m
c_p	Specific heat capacity of air at constant pressure	$J\,kg^{-1}\,K^{-1}$
C	r_{vol}/r_{eff}	1
D, D_c, D_w, D_{IS}	Depth, contrail depth, wake depth, ice-saturation-layer depth	m
D_{H2O}	Diffusivity of vapor in air	$m^2\,s^{-1}$
EA	Total extinction per flight distance	m
EF	Energy forcing, $\int_{lifetime} W\,RF'dt$	$J\,m^{-1}$
EI, EI_{H2O}, EI_{soot}	Mass emission index of water and soot	$kg\,kg^{-1}$
f_c, f_s	Fraction of ice-forming soot particles and of ice particles surviving the wake vortex phase	1
F	Aircraft engine thrust	N
g	Gravity	$m\,s^{-2}$
G	Slope of mixing line	$Pa\,K^{-1}$
I	Total ice mass per contrail length	$kg\,m^{-1}$
IWC	Ice water content	$kg\,m^{-3}$
m_i, m_{soot}	Mass of an ice particle, soot particles	kg
m_F	Fuel consumption per flight distance	$kg\,m^{-1}$
M	Aircraft mass	kg
M_{air}, M_{H2O}	Molar mass of air and water molecules	$kg\,mol^{-1}$
N_{BV}	Brunt–Väisälä frequency	s^{-1}
N^*_{BV}	$N_{BV}t_0$, stratification parameter	1
N_{dil}	Dilution ratio (plume mass per burned fuel mass)	1
n_i, n_{ice}	Local and mean ice particle concentration	m^{-3}
N_{ice}	Total ice particle number per contrail length	m^{-1}
p, p_{ice}, p_{sat}	Pressure, ice saturation pressure, liquid saturation pressure	Pa
PEI, PEI_{ice}, PEI_{soot}	Particle number emission index, apparent PEI for ice, and PEI for soot	kg^{-1}
Q	Fuel combustion heat	$J\,kg^{-1}$
Q_{ext}	Extinction efficiency	1
r_{area}, r_{eff}, r_{vol}	Area, effective, and volume-mean radius	m
RF, RF_{LW}, RF_{SW}	Radiative forcing, longwave RF, and shortwave RF	$W\,m^{-2}$
RF′	Local RF	$W\,m^{-2}$
RH, RHi	Relative humidity for liquid and ice saturation	1
s	Wing span	m
SS	Ice particle surface area time integral, $\int_{lifetime} N_{ice}\pi r^2_{area}dt$	m s
t	Time	s
T	Temperature	K
V	Aircraft airspeed	$m\,s^{-1}$
w_0	Wake vortex velocity scale	$m\,s^{-1}$
W	Contrail width	m
ε_t	Turbulent kinetic energy dissipation rate	$m^2\,s^{-3}$
ε^*_t	Nondimensional dissipation rate	1
η	Overall propulsion efficiency	1
Γ_0	Initial wake vortex circulation	$m^2\,s^{-1}$
λ	Surface temperature climate sensitivity	$K\,W^{-1}\,m^2$
ρ, ρ_{ice}	Air density, ice-bulk density	$kg\,m^{-3}$
τ	Optical depth (at solar wavelengths)	1

and albedo of the Earth–atmosphere system? Also, future cirrus research should find out more about the ice nucleation properties of ice residuals, from both contrails and other cirrus. With respect to aerodynamic contrails, the number of ice particles surviving the wake vortex phase needs to be quantified as a prerequisite to assess its potential climate and precipitation impacts. In situ ice particle measurements in young contrails seem to miss many of the smaller ice particles.

Further research is needed to reduce uncertainties concerning the key parameters listed in Table 3-1. Among other things, this requires complete sets of measurements that allow for constraining model variants. In situ measurements and remote sensing from ground, aircraft, and space instruments are to be combined with data on air traffic and weather for analysis. The contrail formation process from exhaust formation in the engine to the end of the wake vortex phase needs to be investigated in more detail, in particular when discussing alternative fuels. New instruments are required to measure the small-size and small-scale cirrus properties in situ combined with remote sensing of the ambience at contrail scales to determine local and integral contrail properties and cause–effect relationships simultaneously. Representation of ice supersaturation, temperature, wind shear, and vertical motions in NWP and climate models need to be improved. New ideas are needed to account for the complex contrail–climate interactions at scales from local contrail formation to global. The climate impact of contrail cirrus for given radiative forcing properties needs to be better quantified.

Acknowledgments. We are grateful for figures, data, and comments to Darrel Baumgardner, Phil Brown, Donald Delisi, Dave Duda, Klaus Gierens, Volker Grewe, Jim Haywood, Frank Holzäpfel, Nicolas Lamquin, Patrick Minnis, Simon Unterstraßer, Christiane Voigt, Margarita Vázquez-Navarro, and three anonymous reviewers. The authors would like to thank the many sponsors who have provided funding for the monograph: Leibniz Institute for Tropospheric Research (TROPOS), Forschungszentrum Jülich (FZJ), and Deutsches Zentrum für Luft- und Raumfahrt (DLR), Germany; ETH Zurich, Switzerland; National Center for Atmospheric

Research (NCAR), United States; the Met Office, United Kingdom; the University of Illinois, United States; Environment and Climate Change Canada (ECCC); National Science Foundation (NSF), National Aeronautics and Space Administration (NASA), United States; the International Commission on Clouds and Precipitation (ICCP), the European Facility for Airborne Research (EUFAR), and Droplet Measurement Technologies (DMT), United States. NCAR is sponsored by the NSF. Any opinions, findings and conclusions or recommendations expressed in this publication are those of the author(s) and do not necessarily reflect the views of the National Science Foundation.

APPENDIX

List of Symbols

Table 3-A1 provides a list of the symbols used in this chapter.

REFERENCES

Anderson, B. E., W. R. Cofer, D. R. Bagwell, J. W. Barrick, C. H. Hudgins, and K. E. Brunke, 1998: Airborne observations of aircraft aerosol emissions I: Total nonvolatile particle emission indices. *Geophys. Res. Lett.*, **25**, 1689–1692, doi:10.1029/98GL00063.

Anderson, J. D., 2010: *Fundamentals of Aerodynamics*. McGraw Hill, 1106 pp.

Appleman, H., 1953: The formation of exhaust contrails by jet aircraft. *Bull. Amer. Meteor. Soc.*, **34**, 14–20.

Atlas, D., and Z. Wang, 2010: Contrails of small and very large optical depth. *J. Atmos. Sci.*, **67**, 3065–3073, doi:10.1175/2010JAS3403.1.

——, ——, and D. P. Duda, 2006: Contrails to cirrus—Morphology, microphysics, and radiative properties. *J. Appl. Meteor. Climatol.*, **45**, 5–19, doi:10.1175/JAM2325.1.

aufm Kampe, H. J., 1943: Die Physik der Auspuffwolken hinter Flugzeugen (The physics of exhaust clouds behind aircraft). *Luftwissen*, **10**, 171–173.

Bailey, M. P., and J. Hallett, 2009: A comprehensive habit diagram for atmospheric ice crystals: Confirmation from the laboratory, AIRS II, and other field studies. *J. Atmos. Sci.*, **66**, 2888–2899, doi:10.1175/2009JAS2883.1.

Bauer, P., A. Thorpe, and G. Brunet, 2015: The quiet revolution of numerical weather prediction. *Nature*, **525**, 47–55, doi:10.1038/nature14956.

Baum, B. A., A. J. Heymsfield, P. Yang, and S. T. Bedka, 2005: Bulk scattering properties for the remote sensing of ice clouds. Part I: Microphysical data and models. *J. Appl. Meteor.*, **44**, 1885–1895, doi:10.1175/JAM2308.1.

Baumann, R., R. Busen, H. P. Fimpel, C. Kiemle, M. Reinhardt, and M. Quante, 1993: Measurements on contrails of commercial aircraft. Preprints, *Eighth Symp. on Meteorological Observations and Instrumentation*, Anaheim, CA, Amer. Meteor. Soc., 484–489.

Baumgardner, D., and W. A. Cooper, 1994: Airborne measurements in jet contrails: Characterization of the microphysical properties of aircraft wakes and exhausts. *Impact of Emissions from Aircraft and Spacecraft upon the Atmosphere*, U. Schumann, and D. Wurzel, Eds., DLR, 418–423.

Bedka, S. T., P. Minnis, D. P. Duda, T. L. Chee, and R. Palikonda, 2013: Properties of linear contrails in the Northern Hemisphere derived from 2006 Aqua MODIS observations. *Geophys. Res. Lett.*, **40**, 772–777, doi:10.1029/2012GL054363.

Birner, T., A. Dörnbrack, and U. Schumann, 2002: How sharp is the tropopause at midlatitudes? *Geophys. Res. Lett.*, **29,** 45-1–45-4, doi:10.1029/2002gl015142.

Bock, L., and U. Burkhardt, 2016a: The temporal evolution of a long-lived contrail cirrus cluster: Simulations with a global climate model. *J. Geophys. Res. Atmos.*, **121**, 3548–3565, doi:10.1002/2015JD024475.

——, and ——, 2016b: Reassessing properties and radiative forcing of contrail cirrus using a climate model. *J. Geophys. Res. Atmos*, **121**, 9717–9736, doi:10.1002/2016JD025112.

Boies, A. M., and Coauthors, 2015: Particle emission characteristics of a gas turbine with a double annular combustor. *Aerosol Sci. Technol.*, **49**, 842–855, doi:10.1080/02786826.2015.1078452.

Bond, T. C., and Coauthors, 2013: Bounding the role of black carbon in the climate system: A scientific assessment. *J. Geophys. Res. Atmos.*, **118**, 5380–5552, doi:10.1002/jgrd.50171.

Boucher, O., and Coauthors, 2013: Clouds and aerosols. *Climate Change 2013: The Physical Science Basis*, T. F. Stocker, et al., Eds., Cambridge University Press, 571–657.

Brasseur, G. P., and Coauthors, 2016: Impact of aviation on climate: FAA's Aviation Climate Change Research Initiative (ACCRI) Phase II. *Bull. Amer. Meteor. Soc.*, **97**, 561–583, doi:10.1175/BAMS-D-13-00089.1.

Braun-Unkhoff, M., and U. Riedel, 2015: Alternative fuels in aviation. *CEAS Aeronaut. J.*, **6**, 83–93, doi:10.1007/s13272-014-0131-2.

Brewer, A. W., 1946: Condensation trails. *Weather*, **1**, 34–40, doi:10.1002/j.1477-8696.1946.tb00024.x.

——, 2000: The stratospheric circulation: A personal history. *SPARC Newsletter,* No. 15, 28–32. [Available online at http://www.atmosp.physics.utoronto.ca/SPARC/News15/15_Norton.html.]

Brock, C. A., F. Schröder, B. Kärcher, A. Petzold, R. Busen, and M. Fiebig, 2000: Ultrafine particle size distributions measured in aircraft exhaust plumes. *J. Geophys. Res.*, **105**, 26 555–26 567, doi:10.1029/2000JD900360.

Burkhardt, U., and B. Kärcher, 2011: Global radiative forcing from contrail cirrus. *Nat. Climate Change*, **1**, 54–58, doi:10.1038/nclimate1068.

——, ——, M. Ponater, K. Gierens, and A. Gettelman, 2008: Contrail cirrus supporting areas in model and observations. *Geophys. Res. Lett.*, **35**, L16808, doi:10.1029/2008GL034056.

Busen, R., and U. Schumann, 1995: Visible contrail formation from fuels with different sulfur contents. *Geophys. Res. Lett.*, **22**, 1357–1360, doi:10.1029/95GL01312.

Chen, C.-C., and A. Gettelman, 2013: Simulated radiative forcing from contrails and contrail cirrus. *Atmos. Chem. Phys.*, **13**, 12 525–12 536, doi:10.5194/acp-13-12525-2013.

Comstock, J. M., T. P. Ackerman, and D. D. Turner, 2004: Evidence of high ice supersaturation in cirrus clouds using ARM Raman lidar measurements. *Geophys. Res. Lett.*, **31**, L11106, doi:10.1029/2004GL019705.

de Bruin, A., and H. Kannemans, 2004: Analysis of NLR Cessna Citation flight test data for flight test-1 in AWIATOR project. NLR Tech. Rep. AW-NLR-113-010, 101 pp.

De Leon, R. R., M. Krämer, D. S. Lee, and J. C. Thelen, 2012: Sensitivity of radiative properties of persistent contrails to the

ice water path. *Atmos. Chem. Phys.*, **12**, 7893–7901, doi:10.5194/acp-12-7893-2012.

Delisi, D. P., and R. E. Robins, 2000: Short-scale instabilities in trailing wake vortices in a stratified fluid. *AIAA J.*, **38**, 1916–1923, doi:10.2514/2.845.

——, and G. C. Greene, 2009: Experimental measurements of the evolution of a vortex pair in a nonstratified fluid. Part 1: Migration and persistence. *Proc. 47th AIAA Aerospace Sciences Meeting*, Orlando, FL, AIAA, 14, doi:10.2514/6.2009-345.

De Visscher, I., L. Bricteux, and G. Winckelmans, 2013: Aircraft vortices in stably stratified and weakly turbulent atmospheres: Simulation and modeling. *AIAA J.*, **51**, 551–566, doi:10.2514/1.J051742.

Dickson, N. C., K. M. Gierens, H. L. Rogers, and R. L. Jones, 2010: Probabilistic description of ice-supersaturated layers in low resolution profiles of relative humidity. *Atmos. Chem. Phys.*, **10**, 6749–6763, doi:10.5194/acp-10-6749-2010.

Dietmüller, S., and Coauthors, 2016: A new radiation infrastructure for the Modular Earth Submodel System (MESSy, based on version 2.51). *Geosci. Model Dev.*, **9**, 2209–2222, doi:10.5194/gmd-9-2209-2016.

Duda, D. P., and P. Minnis, 2002: Observations of aircraft dissipation trails from GOES. *Mon. Wea. Rev.*, **130**, 398–406, doi:10.1175/1520-0493(2002)130<0398:OOADTF>2.0.CO;2.

——, ——, and L. Nguyen, 2001: Estimates of cloud radiative forcing in contrail clusters using GOES imagery. *J. Geophys. Res.*, **106**, 4927–4937, doi:10.1029/2000JD900393.

——, ——, L. Nyuyen, and R. Palikonda, 2004: A case study of the development of contrail clusters over the Great Lakes. *J. Atmos. Sci.*, **61**, 1132–1146, doi:10.1175/1520-0469(2004)061<1132:ACSOTD>2.0.CO;2.

——, ——, K. Khlopenkov, T. L. Chee, and R. Boeke, 2013: Estimation of 2006 Northern Hemisphere contrail coverage using MODIS data. *Geophys. Res. Lett.*, **40**, 612–617, doi:10.1002/grl.50097.

——, T. Chee, K. Khlopenkov, S. Bedka, and P. Minnis, 2015: Linear contrail coverage and cloud property retrievals from 2012 MODIS imagery over the Northern Hemisphere. *2015 Fall Meeting*, San Francisco, CA, Amer. Geophys. Union., Abstract A11S-03.

Dyroff, C., A. Zahn, E. Christner, R. M. Forbes, A. M. Tompkins, and P. J. van Velthoven, 2015: Comparison of ECMWF analysis and forecast humidity data with CARIBIC upper troposphere and lower stratosphere observations. *Quart. J. Roy. Meteor. Soc.*, **141A**, 833–844, doi:10.1002/qj.2400.

Ewald, F., L. Bugliaro, H. Mannstein, and B. Mayer, 2013: An improved cirrus detection algorithm MeCiDA2 for SEVIRI and its evaluation with MODIS. *Atmos. Meas. Tech.*, **6**, 309–322, doi:10.5194/amt-6-309-2013.

Fahey, D. W., and Coauthors, 1995: Emission measurements of the Concorde supersonic aircraft in the lower stratosphere. *Science*, **270**, 70–74, doi:10.1126/science.270.5233.70.

Febvre, G., and Coauthors, 2009: On optical and microphysical characteristics of contrails and cirrus. *J. Geophys. Res.*, **114**, D02204, doi:10.1029/2008JD010184.

Freudenthaler, V., F. Homburg, and H. Jäger, 1995: Contrail observations by ground-based scanning lidar: Cross-sectional growth. *Geophys. Res. Lett.*, **22**, 3501–3504, doi:10.1029/95GL03549.

——, ——, and ——, 1996: Optical parameters of contrails from lidar measurements: Linear depolarization. *Geophys. Res. Lett.*, **23**, 3715–3718, doi:10.1029/96GL03646.

Frömming, C., M. Ponater, U. Burkhardt, A. Stenke, S. Pechtl, and R. Sausen, 2011: Sensitivity of contrail coverage and contrail radiative forcing to selected key parameters. *Atmos. Environ.*, **45**, 1483–1490, doi:10.1016/j.atmosenv.2010.11.033.

Fuglestvedt, J. S., and Coauthors, 2010: Transport impacts on atmosphere and climate: Metrics. *Atmos. Environ.*, **44**, 4648–4677, doi:10.1016/j.atmosenv.2009.04.044.

Gao, R. C., and Coauthors, 2006: Measurements of relative humidity in a persistent contrail. *Atmos. Environ.*, **40**, 1590–1600, doi:10.1016/j.atmosenv.2005.11.021.

Gayet, J.-F., G. Febvre, G. Brogniez, H. Chepfer, W. Renger, and P. Wendling, 1996: Microphysical and optical properties of cirrus and contrails. *J. Atmos. Sci.*, **53**, 126–138, doi:10.1175/1520-0469(1996)053<0126:MAOPOC>2.0.CO;2.

——, and Coauthors, 2012: The evolution of microphysical and optical properties of an A380 contrail in the vortex phase. *Atmos. Chem. Phys.*, **12**, 6629–6643, doi:10.5194/acp-12-6629-2012.

Gerz, T., and T. Ehret, 1996: Wake dynamics and exhaust distribution behind cruising aircraft. *AGARD Fluid Dynamics Panel Meeting and Symp. on the Characterization and Modification of Wakes from Lifting Vehicles in Fluids*, Trondheim, Norway, AGARD CP 584, 35.31–35.38.

——, and F. Holzäpfel, 1999: Wing tip vortices, turbulence and the distribution of emissions. *AIAA J.*, **37**, 1270–1276, doi:10.2514/2.595.

Gettelman, A., and C. Chen, 2013: The climate impact of aviation aerosols. *Geophys. Res. Lett.*, **40**, 2785–2789, doi:10.1002/grl.50520.

Gierens, K., 2012: Selected topics on the interaction between cirrus clouds and embedded contrails. *Atmos. Chem. Phys.*, **12**, 11 943–11 949, doi:10.5194/acp-12-11943-2012.

——, and P. Spichtinger, 2000: On the size distribution of ice-supersaturated regions in the upper troposphere and lowermost stratosphere. *Ann. Geophys.*, **18**, 499–504, doi:10.1007/s00585-000-0499-7.

——, and S. Brinkop, 2012: Dynamical characteristics of ice supersaturated regions. *Atmos. Chem. Phys.*, **12**, 11 933–11 942, doi:10.5194/acp-12-11933-2012.

——, and F. Dilger, 2013: A climatology of formation conditions for aerodynamic contrails. *Atmos. Chem. Phys.*, **13**, 10 847–10 857, doi:10.5194/acp-13-10847-2013.

——, B. Kärcher, H. Mannstein, and B. Mayer, 2009: Aerodynamic contrails: Phenomenology and flow physics. *J. Atmos. Sci.*, **66**, 217–226, doi:10.1175/2008JAS2767.1.

——, M. Kästner, and D. Klatt, 2011: Iridescent aerodynamic contrails: The Norderney case of 27 June 2008. *Meteor. Z.*, **20**, 305–311, doi:10.1127/0941-2948/2011/0497.

——, P. Spichtinger, and U. Schumann, 2012: Ice supersaturation. *Atmospheric Physics: Background—Methods—Trends*, U. Schumann, Ed., Research Topics in Aerospace Series, Vol. 1, Springer, 135–150, doi:10.1007/978-3-642-30183-4_9.

Graf, K., U. Schumann, H. Mannstein, and B. Mayer, 2012: Aviation induced diurnal North Atlantic cirrus cover cycle. *Geophys. Res. Lett.*, **39**, L16804, doi:10.1029/2012GL052590.

Greene, G. C., 1986: An approximate model of wake vortex decay in the atmosphere. *J. Aircr.*, **23**, 566–573, doi:10.2514/3.45345.

Grewe, V., T. Champougny, S. Matthes, C. Frömming, S. Brinkop, O. A. Søvde, E. A. Irvine, and L. Halscheidt, 2014a: Reduction of the air traffic's contribution to climate change: A REACT4C case study. *Atmos. Environ.*, **94**, 616–625, doi:10.1016/j.atmosenv.2014.05.059.

——, and Coauthors, 2014b: Aircraft routing with minimal climate impact: The REACT4C climate cost function modelling approach (V1.0). *Geosci. Model Dev.*, **7**, 175–201, doi:10.5194/gmd-7-175-2014.

Hansen, J. E., and L. D. Travis, 1974: Light scattering in planetary atmospheres. *Space Sci. Rev.*, **16**, 527–610, doi:10.1007/BF00168069.

——, and Coauthors, 2005: Efficacy of climate forcings. *J. Geophys. Res.*, **110**, D18104, doi:10.1029/2005JD005776.

Haywood, J. M., and Coauthors, 2009: A case study of the radiative forcing of persistent contrails evolving into contrail-induced cirrus. *J. Geophys. Res.*, **114**, D24201, doi:10.1029/2009JD012650.

Helten, M., and Coauthors, 1999: In-flight comparison of MOZAIC and POLINAT water vapor measurements. *J. Geophys. Res.*, **104**, 26 087–26 096, doi:10.1029/1999JD900315.

Hendricks, J., B. Kärcher, and U. Lohmann, 2011: Effects of ice nuclei on cirrus clouds in a global climate model. *J. Geophys. Res.*, **116**, D18206, doi:10.1029/2010JD015302.

Hennemann, I., and F. Holzäpfel, 2011: Large-eddy simulation of aircraft wake vortex deformation and topology. *J. Aerosp. Eng.*, **25**, 1336–1350, doi:10.1177/0954410011402257.

Heymsfield, A. J., R. P. Lawson, and G. W. Sachse, 1998: Growth of ice crystals in a precipitating contrail. *Geophys. Res. Lett.*, **25**, 1335–1338, doi:10.1029/98GL00189.

——, D. Baumgardner, P. DeMott, P. Forster, K. Gierens, and B. Kärcher, 2010: Contrail microphysics. *Bull. Amer. Meteor. Soc.*, **91**, 465–472, doi:10.1175/2009BAMS2839.1.

——, G. Thompson, H. Morrison, A. Bansemer, R. M. Rasmussen, P. Minnis, Z. Wang, and D. Zhang, 2011: Formation and spread of aircraft-Induced holes in clouds. *Science*, **333**, doi:10.1126/science.1202851.

——, C. Schmitt, and A. Bansemer, 2013: Ice cloud particle size distributions and pressure-dependent terminal velocities from in situ observations at temperatures from 0° to −86°C. *J. Atmos. Sci.*, **70**, 4123–4154, doi:10.1175/JAS-D-12-0124.1.

Holzäpfel, F., 2003: Probabilistic two-phase wake vortex decay and transport model. *J. Aircr.*, **40**, 323–331, doi:10.2514/2.3096.

——, 2014: Effects of environmental and aircraft parameters on wake vortex behavior. *J. Aircr.*, **51**, 1490–1500, doi:10.2514/1.C032366.

Hoshizaki, H., L. B. Anderson, R. J. Conti, N. Farlow, J. W. Meyer, T. Overcamp, K. O. Redler, and V. Watson, 1975: Aircraft wake microscale phenomena. *The Stratosphere Perturbed by Propulsion Effluents*, A. J. Grobecker, Ed., Department of Transportation, Climatic Impact Assessment Program, 2-1–2-79.

Immler, F., R. Treffeisen, D. Engelbart, K. Krüger, and O. Schrems, 2008: Cirrus, contrails, and ice supersaturated regions in high pressure systems at northern mid latitudes. *Atmos. Chem. Phys.*, **8**, 1689–1699, doi:10.5194/acp-8-1689-2008.

IPCC, 2013: *Climate Change 2013: The Physical Science Basis*. Cambridge University Press, 1535 pp.

Irvine, E. A., and K. P. Shine, 2015: Ice supersaturation and the potential for contrail formation in a changing climate. *Earth Syst. Dyn.*, **6**, 555–568, doi:10.5194/esd-6-555-2015.

Iwabuchi, H., P. Yang, K. N. Liou, and P. Minnis, 2012: Physical and optical properties of persistent contrails: Climatology and interpretation. *J. Geophys. Res.*, **117**, D06215, doi:10.1029/2011JD017020.

Jansen, J., and A. J. Heymsfield, 2015: Microphysics of aerodynamic contrail formation processes. *J. Atmos. Sci.*, **72**, 3293–3308, doi:10.1175/JAS-D-14-0362.1.

Jensen, E. J., and O. B. Toon, 1997: The potential impact of soot particles from aircraft exhaust on cirrus clouds. *Geophys. Res. Lett.*, **24**, 249–252, doi:10.1029/96GL03235.

——, A. S. Ackermann, D. E. Stevens, O. B. Toon, and P. Minnis, 1998a: Spreading and growth of contrails in a sheared environment. *J. Geophys. Res.*, **103**, 13 557–513 567, doi:10.1029/98JD02594.

——, and Coauthors, 1998b: Environmental conditions required for contrail formation and persistence. *J. Geophys. Res.*, **103**, 3929–3936, doi:10.1029/97JD02808.

——, and Coauthors, 2001: Prevalence of ice-supersaturated regions in the upper troposphere: Implications for optically thin ice cloud formation. *J. Geophys. Res.*, **106**, 17 253–17 266, doi:10.1029/2000JD900526.

Jeßberger, P., and Coauthors, 2013: Aircraft type influence on contrail properties. *Atmos. Chem. Phys.*, **13**, 11 965–11 984, doi:10.5194/acp-13-11965-2013.

Jones, H. M., and Coauthors, 2012: A methodology for in-situ and remote sensing of microphysical and radiative properties of contrails as they evolve into cirrus. *Atmos. Chem. Phys.*, **12**, 8157–8175, doi:10.5194/acp-12-8157-2012.

Jurkat, T., and Coauthors, 2011: Measurements of HONO, NO, NO_y and SO_2 in aircraft exhaust plumes at cruise. *Geophys. Res. Lett.*, **38**, L10807, doi:10.1029/2011GL046884.

Kärcher, B., and F. Yu, 2009: Role of aircraft soot emissions in contrail formation. *Geophys. Res. Lett.*, **36**, L01804, doi:10.1029/2008GL036649.

——, and U. Burkhardt, 2013: Effects of optical depth variability on contrail radiative forcing. *Quart. J. Roy. Meteor. Soc.*, **139**, 1658–1664, doi:10.1002/qj.2053.

——, T. Peter, U. M. Biermann, and U. Schumann, 1996: The initial composition of jet condensation trails. *J. Atmos. Sci.*, **53**, 3066–3083, doi:10.1175/1520-0469(1996)053<3066:TICOJC>2.0.CO;2.

——, B. Mayer, K. Gierens, U. Burkhardt, H. Mannstein, and R. Chatterjee, 2009: Aerodynamic contrails: Microphysics and optical properties. *J. Atmos. Sci.*, **66**, 227–243, doi:10.1175/2008JAS2768.1.

——, U. Burkhardt, A. Bier, L. Bock, and I. J. Ford, 2015: The microphysical pathway to contrail formation. *J. Geophys. Res. Atmos.*, **120**, 7893–7927, doi:10.1002/2015JD023491.

Kaufmann, S., C. Voigt, P. Jeßberger, T. Jurkat, H. Schlager, A. Schwarzenboeck, M. Klingebiel, and T. Thornberry, 2014: In-situ measurements of ice saturation in young contrails. *Geophys. Res. Lett.*, **41**, 702–709, doi:10.1002/2013GL058276.

Khou, J.-C., W. Ghedhaifi, X. Vancassel, and F. Garnier, 2015: Spatial simulation of contrail formation in near-field of commercial aircraft. *J. Aircr.*, **52**, 1927–1938, doi:10.2514/1.C033101.

Khvorostyanov, V., and K. Sassen, 1998: Cloud model simulation of a contrail case study: Surface cooling against upper tropospheric warming. *Geophys. Res. Lett.*, **25**, 2145–2148, doi:10.1029/98GL01522.

Kienast-Sjögren, E., P. Spichtinger, and K. Gierens, 2013: Formulation and test of an ice aggregation scheme for two-moment bulk microphysics schemes. *Atmos. Chem. Phys.*, **13**, 9021–9037, doi:10.5194/acp-13-9021-2013.

Knollenberg, R. G., 1972: Measurements of the growth of the ice budget in a persisting contrail. *J. Atmos. Sci.*, **29**, 1367–1374, doi:10.1175/1520-0469(1972)029<1367:MOTGOT>2.0.CO;2.

Koehler, K. A., and Coauthors, 2009: Cloud condensation nuclei and ice nucleation activity of hydrophobic and hydrophilic soot particles. *Phys. Chem. Chem. Phys.*, **11**, 7906–7920, doi:10.1039/b905334b.

Konopka, P., 1995: Analytical Gaussian solutions for anisotropic diffusion in a linear shear flow. *J. Non-Equilib. Thermodyn.*, **20**, 78–91.

Korolev, A., and I. P. Mazin, 2003: Supersaturation of water vapor in clouds. *J. Atmos. Sci.*, **60**, 2957–2974, doi:10.1175/1520-0469(2003)060<2957:SOWVIC>2.0.CO;2.

——, E. Emery, J. Strapp, S. Cober, G. Isaac, M. Wasey, and D. Marcotte, 2011: Small ice particles in tropospheric clouds: Fact or artifact? Airborne icing instrumentation evaluation experiment. *Bull. Amer. Meteor. Soc.*, **92**, 967–973, doi:10.1175/2010BAMS3141.1.

Kristensson, A., J.-F. Gayet, J. Ström, and F. Auriol, 2000: In situ observations of a reduction in effective crystal diameter in cirrus clouds near flight corridors. *Geophys. Res. Lett.*, **27**, 681–684, doi:10.1029/1999GL010934.

Kuhn, M., A. Petzold, D. Baumgardner, and F. Schröder, 1998: Particle composition of a young condensation trail and of upper tropospheric aerosol. *Geophys. Res. Lett.*, **25**, 2679–2682, doi:10.1029/98GL01932.

Laken, B. A., E. Palla, D. R. Kniveton, C. J. R. Williams, and D. A. Kilham, 2012: Contrails developed under frontal influences of the North Atlantic. *J. Geophys. Res.*, **117**, D11201, doi:10.1029/2011JD017019.

Lamquin, N., C. J. Stubenrauch, K. Gierens, U. Burkhardt, and H. Smit, 2012: A global climatology of upper-tropospheric ice supersaturation occurrence inferred from the Atmospheric Infrared Sounder calibrated by MOZAIC. *Atmos. Chem. Phys.*, **12**, 381–405, doi:10.5194/acp-12-381-2012.

Lee, D. S., and Coauthors, 2010: Transport impacts on atmosphere and climate: Aviation. *Atmos. Environ.*, **44**, 4678–4734, doi:10.1016/j.atmosenv.2009.06.005.

Lewellen, D. C., 2012: Analytic solutions for evolving size distributions of spherical crystals or droplets undergoing diffusional growth in different regimes. *J. Atmos. Sci.*, **69**, 417–434, doi:10.1175/JAS-D-11-029.1.

——, 2014: Persistent contrails and contrail cirrus. Part II: Full lifetime behavior. *J. Atmos. Sci.*, **71**, 4420–4438, doi:10.1175/JAS-D-13-0317.1.

——, and W. S. Lewellen, 2001: The effects of aircraft wake dynamics on contrail development. *J. Atmos. Sci.*, **58**, 390–406, doi:10.1175/1520-0469(2001)058<0390:TEOAWD>2.0.CO;2.

——, O. Meza, and W. W. Huebsch, 2014: Persistent contrails and contrail cirrus. Part I: Large-eddy simulations from inception to demise. *J. Atmos. Sci.*, **71**, 4399–4419, doi:10.1175/JAS-D-13-0316.1.

Liou, K. N., S. C. Ou, and G. Koenig, 1990: An investigation of the climatic effect of contrail cirrus. *Air Traffic and the Environment—Background, Tendencies and Potential Global Atmospheric Effects*, U. Schumann, Ed., Lecture Notes in Engineering, Springer, 154–169.

Liu, X., J. E. Penner, S. J. Ghan, and M. Wang, 2007: Inclusion of ice microphysics in the NCAR Community Atmospheric Model version 3 (CAM3). *J. Climate*, **20**, 4526–4547, doi:10.1175/JCLI4264.1.

Lohmann, U., P. Spichtinger, S. Jess, T. Peter, and H. Smit, 2008: Cirrus cloud formation and ice supersaturated regions in a global climate model. *Environ. Res. Lett.*, **3**, 045022, doi:10.1088/1748-9326/3/4/045022.

Mannstein, H., R. Meyer, and P. Wendling, 1999: Operational detection of contrails from NOAA-AVHRR data. *Int. J. Remote Sens.*, **20**, 1641–1660, doi:10.1080/014311699212650.

——, A. Brömser, and L. Bugliaro, 2010: Ground-based observations for the validation of contrails and cirrus detection in satellite imagery. *Atmos. Meas. Tech.*, **3**, 655–669, doi:10.5194/amt-3-655-2010.

Markowicz, K. M., and M. L. Witek, 2011: Simulations of contrail optical properties and radiative forcing for various crystal shapes. *J. Appl. Meteor. Climatol.*, **50**, 1740–1755, doi:10.1175/2011JAMC2618.1.

Marquart, S., M. Ponater, F. Mager, and R. Sausen, 2003: Future development of contrail cover, optical depth and radiative forcing: Impacts of increasing air traffic and climate change. *J. Climate*, **16**, 2890–2904, doi:10.1175/1520-0442(2003)016<2890:FDOCCO>2.0.CO;2.

Mayer, B., and A. Kylling, 2005: The libRadtran software package for radiative transfer calculations: Description and examples of use. *Atmos. Chem. Phys.*, **5**, 1855–1877, doi:10.5194/acp-5-1855-2005.

Meerkötter, R., U. Schumann, P. Minnis, D. R. Doelling, T. Nakajima, and Y. Tsushima, 1999: Radiative forcing by contrails. *Ann. Geophys.*, **17**, 1080–1094, doi:10.1007/s00585-999-1080-7.

Minnis, P., D. F. Young, D. P. Garber, L. Nguyen, W. L. Smith Jr., and R. Palikonda, 1998: Transformation of contrails into cirrus during SUCCESS. *Geophys. Res. Lett.*, **25**, 1157–1160, doi:10.1029/97GL03314.

——, J. K. Ayers, M. L. Nordeen, and S. P. Weaver, 2003: Contrail frequency over the United States from surface observations. *J. Climate*, **16**, 3447–3462, doi:10.1175/1520-0442(2003)016<3447:CFOTUS>2.0.CO;2.

——, ——, R. Palikonda, and D. Phan, 2004: Contrails, cirrus trends, and climate. *J. Climate*, **17**, 1671–1685, doi:10.1175/1520-0442(2004)017<1671:CCTAC>2.0.CO;2.

——, and Coauthors, 2013: Linear contrail and contrail cirrus properties determined from satellite data. *Geophys. Res. Lett.*, **40**, 3220–3226, doi:10.1002/grl.50569.

Misaka, T., F. Holzäpfel, I. Hennemann, T. Gerz, M. Manhart, and F. Schwertfirm, 2012: Vortex bursting and tracer transport of a counter-rotating vortex pair. *Phys. Fluids*, **24**, 025104, doi:10.1063/1.3684990.

——, ——, and T. Gerz, 2015: Large-eddy simulation of aircraft wake evolution from roll-up until vortex decay. *AIAA J.*, **53**, 2646–2670, doi:10.2514/1.J053671.

Moore, R. H., and Coauthors, 2015: Influence of jet fuel composition on aircraft engine emissions: A synthesis of aerosol emissions data from the NASA APEX, AAFEX, and ACCESS missions. *Energy Fuels*, **29**, 2591–2600, doi:10.1021/ef502618w.

Myhre, G., and Coauthors, 2009: Intercomparison of radiative forcing calculations of stratospheric water vapour and contrails. *Meteor. Z.*, **18**, 585–596, doi:10.1127/0941-2948/2009/0411.

Naiman, A. D., S. K. Lele, and M. Z. Jacobson, 2011: Large eddy simulations of contrail development: Sensitivity to initial and ambient conditions over first twenty minutes. *J. Geophys. Res.*, **116**, D21208, doi:10.1029/2011JD015806.

Ovarlez, J., P. van Velthoven, G. Sachse, S. Vay, H. Schlager, and H. Ovarlez, 2000: Comparison of water vapor measurements from POLINAT2 with ECMWF analyses in high humidity conditions. *J. Geophys. Res.*, **105**, 3737–3744, doi:10.1029/1999JD900954.

——, J. F. Gayet, K. Gierens, J. Ström, H. Ovarlez, F. Auriol, R. Busen, and U. Schumann, 2002: Water vapor measurements inside cirrus clouds in northern and southern hemispheres during INCA. *Geophys. Res. Lett.*, **29**, 60-1–60-4, doi:10.1029/2001gl014440.

Paoli, R., and K. Shariff, 2016: Contrail modeling and simulation. *Annu. Rev. Fluid Mech.*, **48**, 393–427, doi:10.1146/annurev-fluid-010814-013619.

——, L. Nybelen, J. Picot, and D. Cariolle, 2013: Effects of jet/vortex interaction on contrail formation in supersaturated conditions. *Phys. Fluids*, **25**, 053305, doi:10.1063/1.4807063.

——, O. Thouron, J. Escobar, J. Picot, and D. Cariolle, 2014: High-resolution large-eddy simulations of stably stratified flows: Application to subkilometer-scale turbulence in the upper

troposphere–lower stratosphere. *Atmos. Chem. Phys.*, **14**, 5037–5055, doi:10.5194/acp-14-5037-2014.

Peck, J., O. O. Oluwole, H.-W. Wong, and R. C. Miake-Lye, 2013: An algorithm to estimate aircraft cruise black carbon emissions for use in developing a cruise emissions inventory. *J. Air Waste Manage. Assoc.*, **63**, 367–375, doi:10.1080/10962247.2012.751467.

Pedgley, D. E., 2008: Some thoughts on fallstreak holes. *Weather*, **63**, 356–360, doi:10.1002/wea.279.

Penner, J. E., D. H. Lister, D. J. Griggs, D. J. Dokken, and M. McFarland, Eds., 1999: *Aviation and the Global Atmosphere*. Cambridge University Press, 373 pp.

——, Y. Chen, M. Wang, and X. Liu, 2009: Possible influence of anthropogenic aerosols on cirrus clouds and anthropogenic forcing. *Atmos. Chem. Phys.*, **9**, 879–896, doi:10.5194/acp-9-879-2009.

Petzold, A., and Coauthors, 1997: Near-field measurements on contrail properties from fuels with different sulfur content. *J. Geophys. Res.*, **102**, 29 867–29 880, doi:10.1029/97JD02209.

——, and Coauthors, 2013: Recommendations for reporting "black carbon" measurements. *Atmos. Chem. Phys.*, **13**, 8365–8379, doi:10.5194/acp-13-8365-2013.

——, A. Döpelheuer, C. A. Brock, and F. Schröder, 1999: In situ observation and model calculations of black carbon emission by aircraft at cruise altitude. *J. Geophys. Res.*, **104**, 22 171–22 181, doi:10.1029/1999JD900460.

Picot, J., R. Paoli, O. Thouron, and D. Cariolle, 2015: Large-eddy simulation of contrail evolution in the vortex phase and its interaction with atmospheric turbulence. *Atmos. Chem. Phys.*, **15**, 7369–7389, doi:10.5194/acp-15-7369-2015.

Poellot, M. R., W. P. Arnott, and J. Hallett, 1999: In situ observations of contrail microphysics and implications for their radiative impact. *J. Geophys. Res.*, **104**, 12 077–12 084, doi:10.1029/1999JD900109.

Ponater, M., S. Marquart, and R. Sausen, 2002: Contrails in a comprehensive global climate model: Parameterization and radiative forcing results. *J. Geophys. Res.*, **107**, 4164, doi:10.1029/2001JD000429.

——, ——, ——, and U. Schumann, 2005: On contrail climate sensitivity. *Geophys. Res. Lett.*, **32**, L10706, doi:10.1029/2005GL022580.

Rap, A., P. M. Forster, J. M. Haywood, A. Jones, and O. Boucher, 2010a: Estimating the climate impact of linear contrails using the UK Met Office climate model. *Geophys. Res. Lett.*, **37**, L20703, doi:10.1029/2010GL045161.

——, ——, A. Jones, O. Boucher, J. M. Haywood, N. Bellouin, and R. R. D. Leon, 2010b: Parameterization of contrails in the UK Met Office Climate Model. *J. Geophys. Res.*, **115**, D10205, doi:10.1029/2009JD012443.

Rojo, C., X. Vancassel, P. Mirabel, J.-L. Ponche, and F. Garnier, 2015: Impact of alternative jet fuels on aircraft-induced aerosols. *Fuels*, **144**, 335–341, doi:10.1016/j.fuel.2014.12.021.

Ryan, A. C., A. R. MacKenzie, S. Watkins, and R. Timmis, 2011: World War II contrails: A case study of aviation-induced cloudiness. *Int. J. Climatol.*, **32**, 1745–1753, doi:10.1002/joc.2392.

Sarpkaya, T., 1983: Trailing vortices in homogeneous and density stratified media. *J. Fluid Mech.*, **136**, 85–109, doi:10.1017/S0022112083002074.

Sassen, K., 1979: Iridescence in an aircraft contrail. *J. Opt. Soc. Amer.*, **69**, 1080–1083, doi:10.1364/JOSA.69.001080.

Sausen, R., K. Gierens, M. Ponater, and U. Schumann, 1998: A diagnostic study of the global distribution of contrails. Part I: Present day climate. *Theor. Appl. Climatol.*, **61**, 127–141, doi:10.1007/s007040050058.

Schäuble, D., and Coauthors, 2009: Airborne measurements of the nitric acid partitioning in persistent contrails. *Atmos. Chem. Phys.*, **9**, 8189–8197, doi:10.5194/acp-9-8189-2009.

Schröder, F. P., B. Kärcher, A. Petzold, R. Baumann, R. Busen, C. Hoell, and U. Schumann, 1998: Ultrafine aerosol particles in aircraft plumes: In situ observations. *Geophys. Res. Lett.*, **25**, 2789–2792, doi:10.1029/98GL02078.

——, and Coauthors, 2000: The transition of contrails into cirrus clouds. *J. Atmos. Sci.*, **57**, 464–480, doi:10.1175/1520-0469(2000)057<0464:OTTOCI>2.0.CO;2.

Schumann, U., 1996: On conditions for contrail formation from aircraft exhausts. *Meteor. Z.*, **5**, 4–23.

——, 2002: Contrail cirrus. *Cirrus*, D. K. Lynch et al., Eds., Oxford University Press, 231–255.

——, 2005: Formation, properties and climate effects of contrails. *C. R. Phys.*, **6**, 549–565, doi:10.1016/j.crhy.2005.05.002.

——, 2012: A contrail cirrus prediction model. *Geosci. Model Dev.*, **5**, 543–580, doi:10.5194/gmd-5-543-2012.

——, and P. Wendling, 1990: Determination of contrails from satellite data and observational results. *Air Traffic and the Environment—Background, Tendencies and Potential Global Atmospheric Effects*, U. Schumann, Ed., Lecture Notes in Engineering, Springer-Verlag, 138–153.

——, and K. Graf, 2013: Aviation-induced cirrus and radiation changes at diurnal timescales. *J. Geophys. Res. Atmos.*, **118**, 2404–2421, doi:10.1002/jgrd.50184.

——, J. Ström, R. Busen, R. Baumann, K. Gierens, M. Krautstrunk, F. P. Schröder, and J. Stingl, 1996: In situ observations of particles in jet aircraft exhausts and contrails for different sulfur-containing fuels. *J. Geophys. Res.*, **101**, 6853–6870, doi:10.1029/95JD03405.

——, H. Schlager, F. Arnold, R. Baumann, P. Haschberger, and O. Klemm, 1998: Dilution of aircraft exhaust plumes at cruise altitudes. *Atmos. Environ.*, **32**, 3097–3103, doi:10.1016/S1352-2310(97)00455-X.

——, R. Busen, and M. Plohr, 2000: Experimental test of the influence of propulsion efficiency on contrail formation. *J. Aircr.*, **37**, 1083–1087, doi:10.2514/2.2715.

——, and Coauthors, 2002: Influence of fuel sulfur on the composition of aircraft exhaust plumes: The experiments SULFUR 1-7. *J. Geophys. Res.*, **107**, 4247, doi:10.1029/2001JD000813.

——, B. Mayer, K. Gierens, S. Unterstrasser, P. Jessberger, A. Petzold, C. Voigt, and J.-F. Gayet, 2011: Effective radius of ice particles in cirrus and contrails. *J. Atmos. Sci.*, **68**, 300–321, doi:10.1175/2010JAS3562.1.

——, K. Graf, H. Mannstein, and B. Mayer, 2012a: Contrails: Visible aviation induced climate impact. *Atmospheric Physics: Background—Methods—Trends*, U. Schumann, Ed., Research Topics in Aerospace Series, Vol. 1, Springer, 239–257, doi:10.1007/978-3-642-30183-4_15.

——, B. Mayer, K. Graf, and H. Mannstein, 2012b: A parametric radiative forcing model for contrail cirrus. *J. Appl. Meteor. Climatol.*, **51**, 1391–1406, doi:10.1175/JAMC-D-11-0242.1.

——, R. Hempel, H. Flentje, M. Garhammer, K. Graf, S. Kox, H. Lösslein, and B. Mayer, 2013a: Contrail study with ground-based cameras. *Atmos. Meas. Tech.*, **6**, 3597–3612, doi:10.5194/amt-6-3597-2013.

——, P. Jeßberger, and C. Voigt, 2013b: Contrail ice particles in aircraft wakes and their climatic importance. *Geophys. Res. Lett.*, **40**, 2867–2872, doi:10.1002/grl.50539.

——, J. E. Penner, Y. Chen, C. Zhou, and K. Graf, 2015: Dehydration effects from contrails in a coupled contrail-climate

model. *Atmos. Chem. Phys.*, **15**, 11 179–11 199, doi:10.5194/acp-15-11179-2015.

——, and Coauthors, 2017: Properties of individual contrails: A compilation of observations and some comparisons. *Atmos. Chem. Phys.*, **17**, 403–438, doi:10.5194/acp-17-403-2017.

Scorer, R. S., and L. J. Davenport, 1970: Contrails and aircraft downwash. *J. Fluid Mech.*, **43**, 451–464, doi:10.1017/S0022112070002501.

Sharman, R. D., S. B. Trier, T. P. Lane, and J. D. Doyle, 2012: Sources and dynamics of turbulence in the upper troposphere and lower stratosphere: A review. *Geophys. Res. Lett.*, **39**, L12803, doi:10.1029/2012GL051996.

Smit, H. G. J., S. Rohs, P. Neis, D. Boulanger, M. Krämer, A. Wahner, and A. Petzold, 2014: Reanalysis of upper troposphere humidity data from the MOZAIC programme for the period 1994 to 2009. *Atmos. Chem. Phys.*, **14**, 13 241–13 255, doi:10.5194/acp-14-13241-2014.

Spichtinger, P., and M. Leschner, 2016: Horizontal scales of ice-supersaturated regions. *Tellus*, **68B**, 29020, doi:10.3402/tellusb.v68.29020.

——, K. Gierens, and A. Dörnbrack, 2005: Formation of ice supersaturation by mesoscale gravity waves. *Atmos. Chem. Phys.*, **5**, 1243–1255, doi:10.5194/acp-5-1243-2005.

Spinhirne, J. D., W. D. Hart, and D. P. Duda, 1998: Evolution of the morphology and microphysics of contrail cirrus from airborne remote sensing. *Geophys. Res. Lett.*, **25**, 1153–1156, doi:10.1029/97GL03477.

Stettler, M. E. J., A. M. Boies, A. Petzold, and S. R. H. Barrett, 2013: Global civil aviation black carbon emissions. *Environ. Sci. Technol.*, **47**, 10 397–10 404, doi:10.1021/es401356v.

Stordal, F., G. Myhre, E. J. G. Stordal, W. B. Rossow, D. S. Lee, W. Arlander, and T. Svendby, 2005: Is there a trend in cirrus cloud cover due to aircraft traffic? *Atmos. Chem. Phys.*, **5**, 2155–2162, doi:10.5194/acp-5-2155-2005.

Ström, J., and S. Ohlsson, 1998: In situ measurements of enhanced crystal number densities in cirrus clouds caused by aircraft exhaust. *J. Geophys. Res.*, **103**, 11 355–11 362, doi:10.1029/98JD00807.

Stuber, N., M. Ponater, and R. Sausen, 2005: Why radiative forcing might fail as a predictor of climate change. *Climate Dyn.*, **24**, 497–510, doi:10.1007/s00382-004-0497-7.

Sussmann, R., 1997: Optical properties of contrail-induced cirrus: Discussion of unusual halo phenomena. *Appl. Opt.*, **36**, 4195–4201, doi:10.1364/AO.36.004195.

——, and K. Gierens, 1999: Lidar and numerical studies on the different evolution of vortex pair and secondary wake in young contrails. *J. Geophys. Res.*, **104**, 2131–2142, doi:10.1029/1998JD200034.

——, and ——, 2001: Differences in early contrail evolution of two-engine versus four-engine aircraft: Lidar measurements and numerical simulations. *J. Geophys. Res.*, **106**, 4899–4911, doi:10.1029/2000JD900533.

Thuman, W. C., and E. Robinson, 1954: Studies of Alaskan ice-fog particles. *J. Meteor.*, **11**, 151–156, doi:10.1175/1520-0469(1954)011<0151:SOAIFP>2.0.CO;2.

Timko, M. T., and Coauthors, 2010: Gas turbine engine emissions—Part II: Chemical properties of particulate matter. *J. Eng. Gas Turbines Power*, **132**, 061505, doi:10.1115/1.4000132.

Tompkins, A., K. Gierens, and G. Rädel, 2007: Ice supersaturation in the ECMWF Integrated Forecast System. *Quart. J. Roy. Meteor. Soc.*, **133**, 53–63, doi:10.1002/qj.14.

Unterstrasser, S., 2016: Properties of young contrails—A parametrisation based on large-eddy simulations. *Atmos. Chem. Phys.*, **16**, 2059–2082, doi:10.5194/acp-16-2059-2016.

——, and K. Gierens, 2010a: Numerical simulations of contrail-to-cirrus transition—Part 1: An extensive parametric study. *Atmos. Chem. Phys.*, **10**, 2017–2036, doi:10.5194/acp-10-2017-2010.

——, and ——, 2010b: Numerical simulations of contrail-to-cirrus transition—Part 2: Impact of initial ice crystal number, radiation, stratification, secondary nucleation and layer depth. *Atmos. Chem. Phys.*, **10**, 2037–2051, doi:10.5194/acp-10-2037-2010.

——, and I. Sölch, 2012: Numerical modeling of contrail cluster formation. *Proc. Third Int. Conf. on Transport, Atmosphere and Climate (TAC-3)*, Prien am Chiemsee, Germany, DLR, 114–119.

——, and N. Görsch, 2014: Aircraft-type dependency of contrail evolution. *J. Geophys. Res. Atmos.*, **119**, 14 015–14 027, doi:10.1002/2014JD022642.

——, I. Sölch, and K. Gierens, 2012: Cloud resolving modeling of contrail evolution. *Atmospheric Physics: Background—Methods—Trends*, U. Schumann, Ed., Research Topics in Aerospace Series, Vol. 1, Springer, 543–559, doi:10.1007/978-3-642-30183-4_33.

Vázquez-Navarro, M., H. Mannstein, and S. Kox, 2015: Contrail life cycle and properties from 1 year of MSG/SEVIRI rapid-scan images. *Atmos. Chem. Phys.*, **15**, 8739–8749, doi:10.5194/acp-15-8739-2015.

Voigt, C., and Coauthors, 2010: In-situ observations of young contrails—Overview and selected results from the CONCERT campaign. *Atmos. Chem. Phys.*, **10**, 9039–9056, doi:10.5194/acp-10-9039-2010.

——, and Coauthors, 2011: Extinction and optical depth of contrails. *Geophys. Res. Lett.*, **38**, L11806, doi:10.1029/2011GL047189.

——, and Coauthors, 2016: ML-CIRRUS—The airborne experiment on natural cirrus and contrail cirrus with the high-altitude long-range research aircraft HALO. *Bull. Amer. Meteor. Soc.*, doi:10.1175/BAMS-D-15-00213.1.

Weickmann, H., 1945: Formen und Bildung atmosphärischer Eiskristalle. *Beitr. Phys Atmos.*, **28**, 12–52.

Wong, H.-W., and R. C. Miake-Lye, 2010: Parametric studies of contrail ice particle formation in jet regime using microphysical parcel modeling. *Atmos. Chem. Phys.*, **10**, 3261–3272, doi:10.5194/acp-10-3261-2010.

Wu, Y., and O. Pauluis, 2015: What is the representation of the moisture–tropopause relationship in CMIP5 models? *J. Climate*, **28**, 4877–4889, doi:10.1175/JCLI-D-14-00543.1.

Xie, Y., P. Yang, K.-N. Liou, P. Minnis, and D. P. Duda, 2012: Parameterization of contrail radiative properties for climate studies. *Geophys. Res. Lett.*, **39**, L00F02, doi:10.1029/2012GL054043.

Yang, P., K. N. Liou, L. Bi, C. Liu, B. Q. Yi, and B. A. Baum, 2015: On the radiative properties of ice clouds: Light scattering, remote sensing, and radiation parameterization. *Adv. Atmos. Sci.*, **32**, 32–63, doi:10.1007/s00376-014-0011-z.

Zhou, C., and J. E. Penner, 2014: Aircraft soot indirect effect on large-scale cirrus clouds: Is the indirect forcing by aircraft soot positive or negative? *J. Geophys. Res. Atmos.*, **119**, 11 303–11 320, doi:10.1002/2014JD021914.